Composite Structures 288 (2022) 115423

Contents lists available at ScienceDirect

Composite Structures

journal homepage: www.elsevier.com/locate/compstruct

Application of a dynamic thermoelastic coupled model for an aerospace aluminium composite panel

Olga A. Ganilova [a,*], Matthew P. Cartmell [a], Andrew Kiley [b]

[a] Aerospace Centre of Excellence, Department of Mechanical & Aerospace Engineering, University of Strathclyde, Glasgow G1 1XJ, Scotland, UK
[b] Airbus Defence & Space Ltd., Gunnels Wood Road, Stevenage, Hertfordshire SG1 2AS, UK

ARTICLE INFO

Keywords:
Thermoelastic
Thermomechanical
Coupled model
Dynamic
Sandwich plate, aluminum

ABSTRACT

An analytical-numerical coupled model has been derived to predict the effects of dynamic thermo-mechanical loading on aluminium composite panels specifically in the form of metallic skin sandwich structures, for the purposes of enhanced design of spacecraft structures where the environmental conditions comprise combined mechanical and thermal loading. The mechanical loading can arise as a consequence of localised structural dynamics, and the thermal loading is attributable principally to the effects of solar irradiation and eclipse during a satellite's orbit, and together they have the potential to influence de-point adversely, in particular. On this basis a combined physics model is required to deal with the generalised thermoelastic problem and this paper reports on the theoretical work done to achieve that. The research has considered the literature in detail and a refined model has been proposed for an aerospace application which results in an analytical-numerical solution for the thermoelastic problem in aluminium composite panels. The model is explored for a panel under a range of centrally located static mechanical loads, in conjunction with thermal loading provided in the form of various controlled and elevated environmental temperature functions, all for prescribed physical boundary conditions. Both forms of loading are shown to influence the displacement of the panel significantly, thereby confirming the importance of a combined physics model for analysing structures in this context.

1. Introduction

The materials used on the exterior of spacecraft are subjected to many environmental threats that can degrade them, including the vacuum of space itself, solar ultraviolet (UV) radiation, ionising charged particle radiation, plasma, surface charging and arcing, temperature extremes, thermal cycling, impacts from micrometeoroids and orbital debris (MMOD), and environment-induced contamination. In terms of material degradation in space, low-Earth orbit (LEO), defined as the region from 200 to 1000 km above the Earth's surface, is a particularly harsh environment because of the presence of atomic oxygen (AO) along with the threats just mentioned [1]. The environmental challenges of space to a spacecraft component vary in their influence mainly due to the component's material properties, its geometry, and the stresses that it undergoes during normal duty. As a spacecraft moves in and out of eclipse during its orbit around Earth, the degree to which its materials experience thermal cycling temperature extremes depends on their thermo-optical properties (solar absorptance and thermal emittance), the view of the sun, the view of Earth, the view of other surfaces of the spacecraft, the durations of time in sunlight and in shadow, their thermal masses and the influences of equipment or components that produce heat [1]. At the extreme end of operation the cyclic temperature variations can be from −120 °C to +120 °C, and high solar absorptance with low infrared emittance can contribute to such temperature swings in the absence of a spacecraft thermal control system. Sixteen thermal cycles a day, taking the case of the ISS which orbits Earth approximately once every 92 min, may lead to cracking, peeling, spalling or the formation of pinholes in the coating, which then allow AO to start to attack the underlying material [1].

The main forms of environmental heating on orbit are sunlight, sunlight reflected from Earth, a planet, or the Moon, and infrared energy emitted from Earth. During launch or in exceptionally low orbits, there is also a free molecular heating effect caused by friction in the rarified upper atmosphere [2]. The main conditions of LEO that are highlighted are the temperature extremes and the thermal cycles experienced throughout the orbit, with a spacecraft completing from eleven to sixteen thermal cycles daily, within a possible temperature range of −120 °C to +120 °C. The thermo-optical properties of the spacecraft

* Corresponding author.
E-mail address: olga.ganilova@strath.ac.uk (O.A. Ganilova).

https://doi.org/10.1016/j.compstruct.2022.115423
Received 24 June 2021; Received in revised form 17 February 2022; Accepted 22 February 2022
Available online 26 February 2022

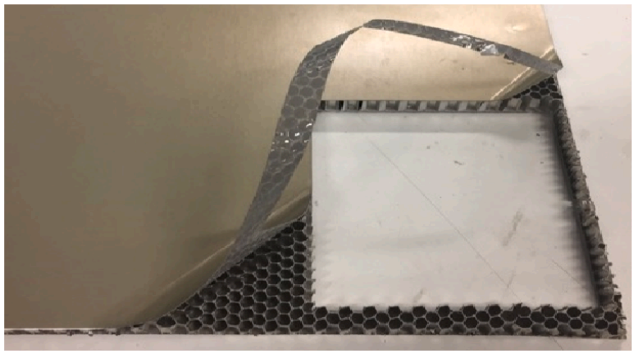

Fig. 1. Honeycomb sandwich panel typically used in the aerospace industry.

Table 1
Mechanical properties of sandwich panel.

	Al-2024	Al-50563/16 Honeycomb
Density, ρ (kg/m^3)	2780	50
Young's Modulus, E (Pa)	73.1×10^9	669×10^6
Shear Modulus, G (Pa)	27.5×10^9	310×10^6
Poisson's Ratio, ν	0.33	0.3
Foil thickness (m [in])		0.0254×10^{-3} [0.001]

Table 2
Thermal properties of sandwich panel skin and honeycomb materials.

	Al-2024	Al-5056
Coefficient of Thermal Expansion (/°C)	2.47×10^{-5}	2.41×10^{-5}
Coefficient of Thermal Expansion for 3/16 honeycomb (/°C)		2.4×10^{-6}
Thermal Conductivity @ 25 °C (W/mK)	149	209
Specific Heat (J/kg°C)	875	904

play a factor in the temperature that it reaches. For instance, a material with high solar absorptance and low thermal emittance will experience greater temperature swings.

In [3] an experiment was performed to investigate the thermal behaviour of a sandwich plate or panel deployable as an integral part of a satellite in a space environment using a ground thermal-vacuum test. It was highlighted that the heat sink, solar radiation, infrared radiation of the Earth, heat conduction, surface radiation and cavity radiation would all influence the temperature field, and the conclusion was that these combined effects would result in a serious challenge for thermal testing in the laboratory of the simulated space environment. The experiment was relatively sophisticated and satisfied the general requirements of the inclusion of three key conditions: ultra-high level of vacuum (lower than 10^{-5} Pa), a heat sink (−180 °C) achieved in this case by using black panels with a liquid-nitrogen cooling system, and thermal loading, achieved through infrared lamps. An interesting study carried out by [4] focused on the effect of thermal cycling in a simulated LEO environment on the microhardness of aluminium alloys, and subjected these alloys to thermal cycles ranging from −140 °C to +110 °C. This was in order to induce thermal fatigue and to study the resulting stress state and mechanical properties of the material. The testing resulted in cyclic plastic deformation which was found to lead to crack initiation, identified using a transmission electron microscope (TEM). A total of 400 thermal cycles was imposed on the samples which showed an eventual decrease in hardness that, from 300 to 400 cycles, then increased with every cycle. Although rapid temperature changes were implied, the exact value of the rate of change of temperature was not stated in the study. The mechanical load was applied at intervals to test the microhardness of the material and was not applied in conjunction with the change in temperature. The study concluded that aluminium alloys exposed to extended thermal cycling (typically of the order of 400 cycles) exhibited obvious softening behaviour, causing phase transformations that, if the cycles were to continue, would lead to crack initiation. The principal finding from this work was that the bulk of aeronautical materials that undergo periodic heating and cooling can be damaged to varying degrees, with thermal fatigue having a great impact on the mechanical properties of the materials used. Although it is difficult to recreate terrestrially the conditions of low Earth orbit, such work has been attempted in the past by [5]. The study focused on subjecting graphite-epoxy composites to the conditions of low Earth orbit. Not only did the materials undergo thermal cycling similar to that experienced in LEO, but the environment was also in a high vacuum state while the effect of ultraviolet radiation was applied during heating but not during cooling. A single thermal cycle was judged to be from −70 °C to +100 °C and back to −70 °C again. This was with a temperature change rate of 3–5 °C/min and a dwell-time at the temperature extremes of 15 min, giving an average cycle time of 100 min, typical of a low Earth orbital period. The results examined were for composites subjected to this environment for 8, 16, 40 and 80 thermal cycles in which the transverse flexural strength and transverse tensile strength showed the most severe reduction with thermal cycling, with losses of 34% and 21% respectively, after 80 thermal cycles. It was considered that the matrix-dominated mechanical properties suffered the greatest loss because of the loss of the matrix due to high vacuum and thermal cycling. Overall, the strength and stiffness of the graphite epoxy composites was shown to decrease exponentially with increasing thermal cycles. Further work into the synergistic effects of high vacuum and thermal cycling was implemented by [6], this time on carbon fibre epoxy composites. The experiment took place in a high vacuum state of 10^{-5} Torr where a single thermal cycle was judged to be from +120 °C to −175 °C and back to +120 °C, over a duration of approximately 43 min. The experiment ran for 500, 1000, 1500 and 2000 cycles. Panels were then subjected to mechanical tests at an ambient temperature of 23 °C to observe the mechanical properties of the samples. The results confirmed gradual damage with the progression of thermal cycles. This was coupled with the degradation of the fibre-matrix interface due to a weakened fibre-matrix bond which led to interfacial sliding.

Some industrial experiments involving the thermal loading of aluminium composite panels, but not using temperatures as extreme as those experienced in low Earth orbit, measured thermo-elastic

Table 3
Dimensions of Sandwich Panel Sample.

Length, a (x10^{-3} m)	Width, b (x10^{-3} m)	Face Thickness (x10^{-3} m)	Honeycomb layer thickness (x10^{-3} m)	HoneycombCell size (m)	Foil Thickness (m)
300	100	0.38	14.24	0.0048(3/16 in)	2.54 x10^{-5} *m*(0.001 in)

Table 4
Maximum actual displacement presented in [26] at maximum mechanical loading of 160 N.

Temperature of environment (°C)	**100**	**80**	**60**	**40**	**20**	**−20**	**−40**	**−60**	**−100**	**−150**
Maximum displacement (x10^{-3} m)	0.7	0.5	0.45	0.45	0.4	0.3	0.3	0.25	0.25	0.2

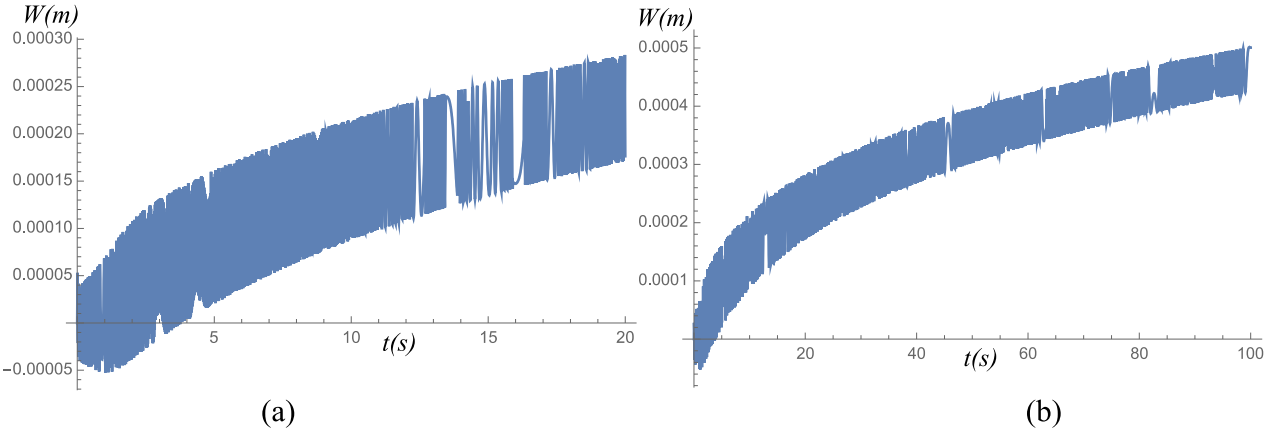

Fig. 2. Displacement response in the time domain when subjected to increasing mechanical loading (a) up to 160 N at 16 s and (b) – further loading in time, within an environmental temperature of *100 °C*.

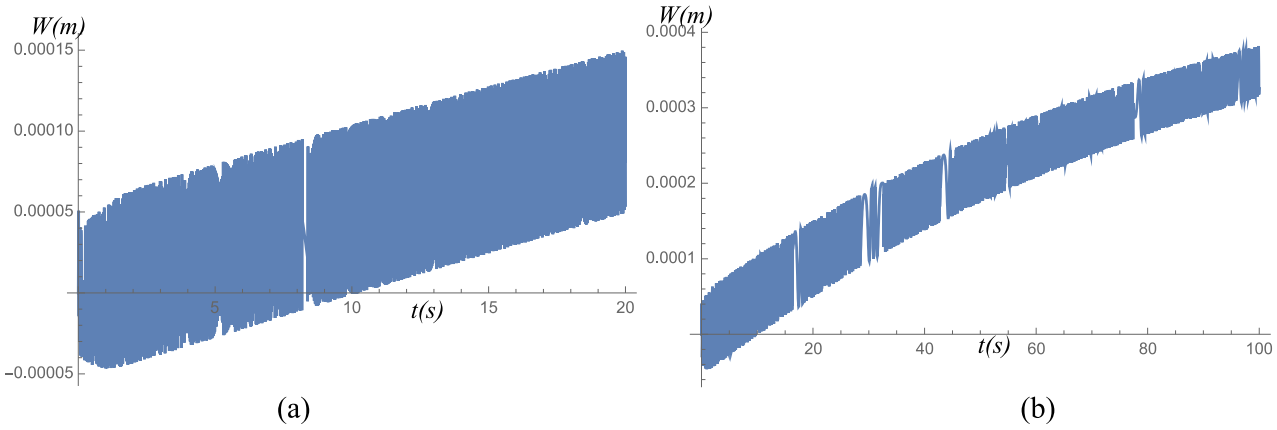

Fig. 3. Displacement response in the time domain when subjected to increasing mechanical loading (a) up to 160 N at 16 s and (b) – further loading in time, within an environmental temperature of *80 °C*.

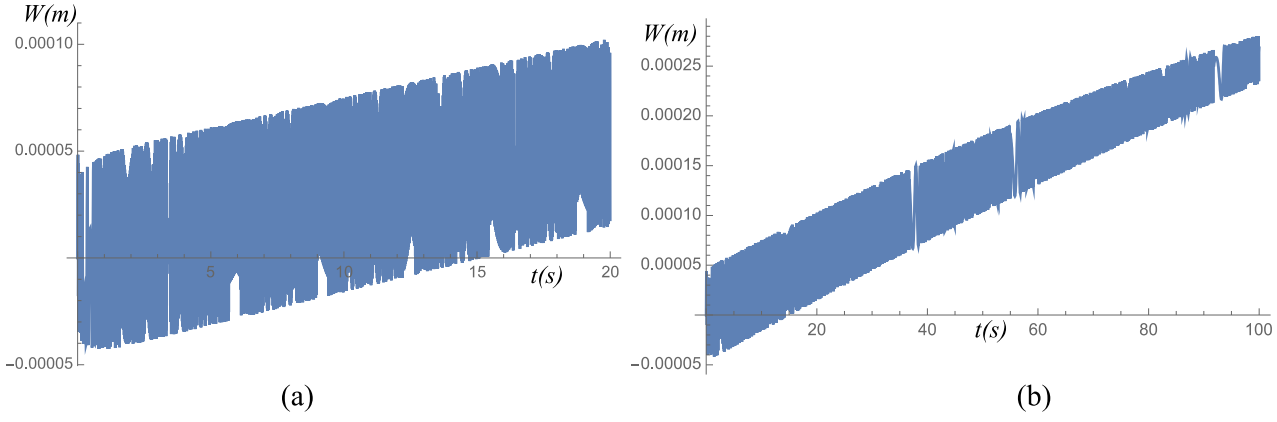

Fig. 4. Displacement response in the time domain when subjected to increasing mechanical loading (a) up to 160 N at 16 s and (b) – further loading in time, within an environmental temperature of *60 °C*.

deformation under thermal load with temperature steps from −20 °C to +40 °C with static loads imposed on the panel between 0 and 78 N – in steps of 19.6 N. The experiment was carried out in a climatic chamber with the measurements being corroborated by a finite element model. Measurements for the deflection and sample temperature of the structural model were taken at set temperatures using photogrammetry and infrared cameras to map a thermal cartographic image of the structural model, where temperatures were assumed as for black body conditions (emissivity, $\varepsilon = 1$). Looking at the problem of a spacecraft panel undergoing *cyclic loading* from the perspective of modelling it is possible to find that the structure must combine the effects of thermal loading as well as mechanical disturbance. This is because from a physical point of view the deformation of a body is connected to a change of heat inside it, and therefore to a change in the temperature distribution in the body.

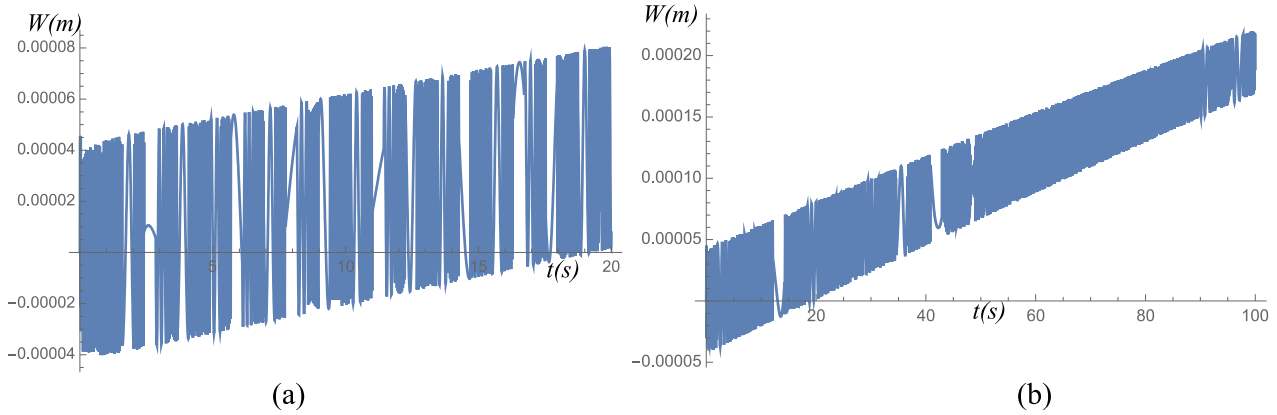

Fig. 5. Displacement response in the time domain when subjected to increasing mechanical loading (a) up to 160 N at 16 s and (b) – further loading in time, within an environmental temperature of *40 °C*.

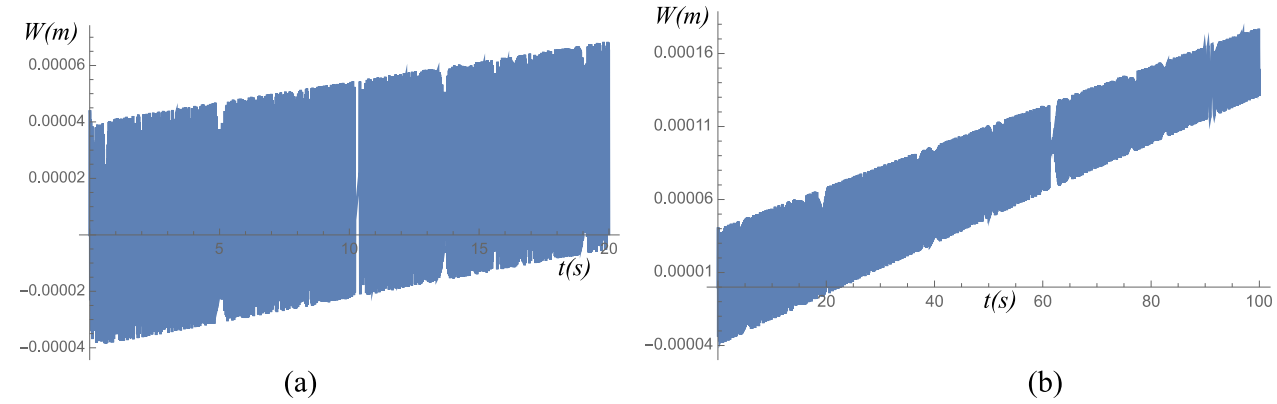

Fig. 6. Displacement response in the time domain when subjected to increasing mechanical loading (a) up to 160 N at 16 s and (b) – further loading in time, within an environment of ambient temperature.

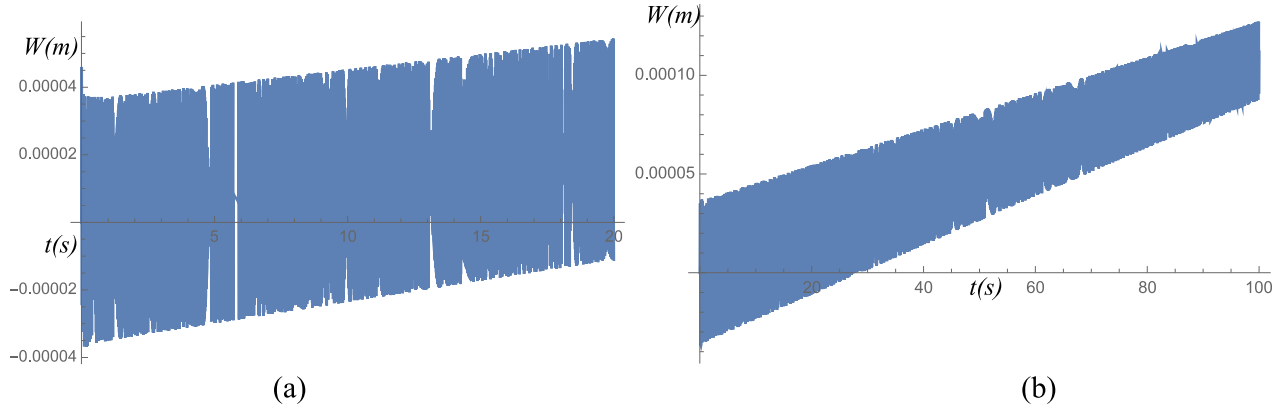

Fig. 7. Displacement response in the time domain when subjected to increasing mechanical loading (a) up to 160 N at 16 s and (b) – further loading in time, within an environmental temperature of *−20 °C*.

So, *a deformation of the body leads to temperature changes, and conversely*. The internal energy of the body depends on both the temperature and the deformation and so, in the case of a practical body, such as a spacecraft panel, this necessarily undergoes processes that are intrinsically coupled, defined collectively as thermoelasticity [7]. In order to summarise, the theory of thermal stresses (TTS) commonly applies a simplifying assumption that the influence of the deformation on the temperature field may be neglected [7]. In TTS the classical heat conduction (HC) equation is usually used but this does not routinely contain the term representing the deformation of the body. Knowing the temperature distribution from the solution of the HC equation, the displacement equations of the theory of elasticity can be solved. At the same time classical dynamic elasticity has been developed under the assumption that the heat exchange between different parts of the body due to the heat conduction occurs very slowly, and therefore the thermal motion may be regarded as *adiabatic*.

However, thermoelasticity deals with a wide class of phenomena. It covers the general theory of heat conduction as well as the general

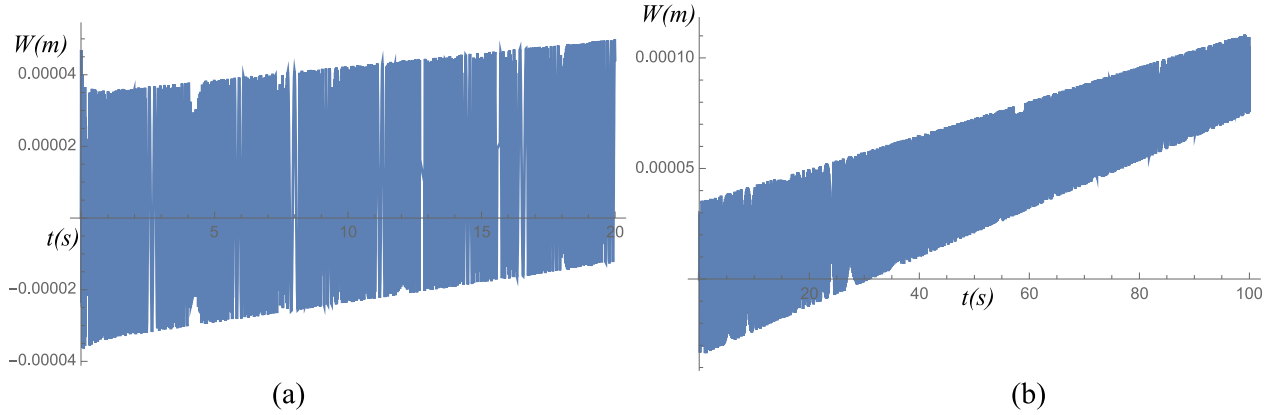

Fig. 8. Displacement response in the time domain when subjected to increasing mechanical loading (a) up to 160 N at 16 s and (b) – further loading in time, within an environmental temperature of $-40\ ^{\circ}C$.

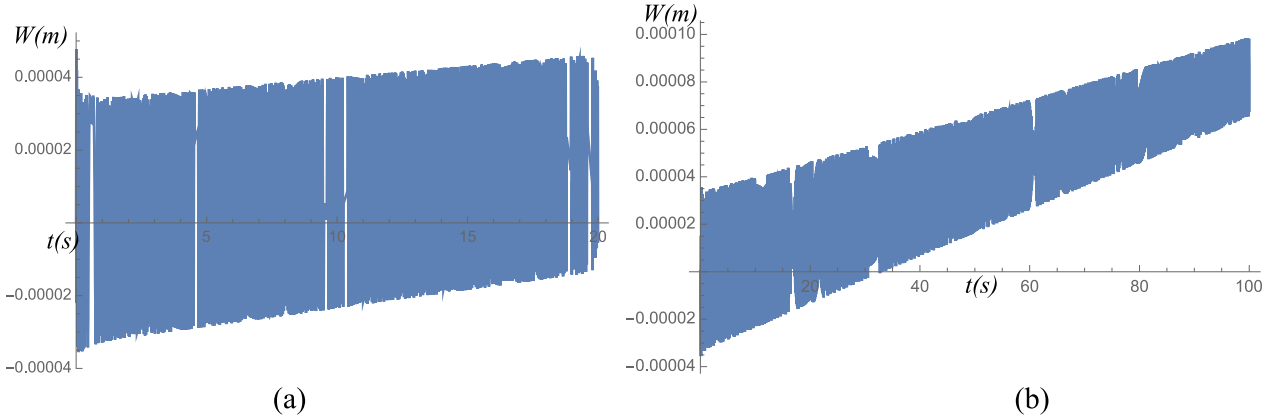

Fig. 9. Displacement response in the time domain when subjected to increasing mechanical loading (a) up to 160 N at 16 s and (b) – further loading in time, within an environmental temperature of $-60\ ^{\circ}C$.

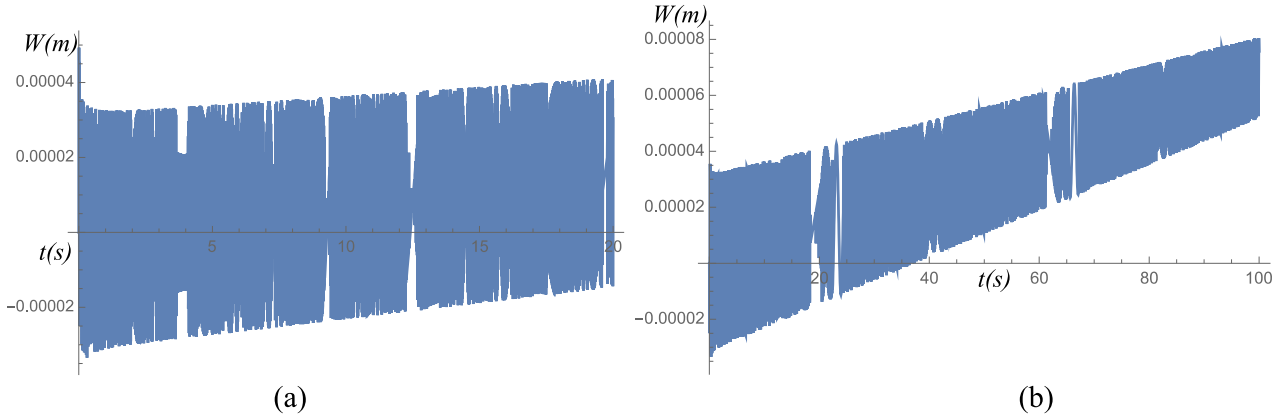

Fig. 10. Displacement response in the time domain when subjected to increasing mechanical loading (a) up to 160 N at 16 s and (b) – further loading in time, within an environmental temperature of $-100\ ^{\circ}C$.

theory of thermal stresses, and it describes the temperature distribution produced by deformation. Thermoelasticity also describes the phenomenon of thermoelastic dissipation. As mentioned above many modelling approaches tend to separate the mechanical and thermal effects, but thermoelastic processes are not generally reversible because although the elastic part may be reversed - the deformations may be recoverable through cooling - the thermal part may not be reversed due to the dissipation of energy during heat transfer [8].

Apart from that, thermal changes in the body cause mechanical deformation in the body, which in return affects these thermal changes, representing the process as two-way feedback, and this mechanism is at the heart of the current work presented in this paper. To do this properly requires that the modelling techniques and representations really do have to couple the mechanical and thermal aspects of the problem to achieve results of meaningful accuracy. A literature review of commonly used techniques for thermoelastic problems is presented in [8]. It was

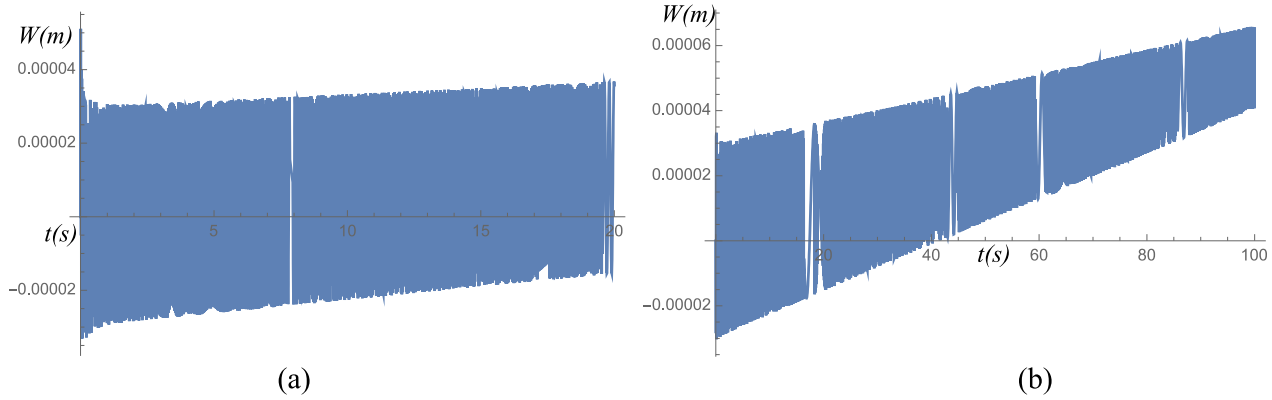

Fig. 11. Displacement response in the time domain when subjected to increasing mechanical loading (a) up to 160 N at 16 s and (b) – further loading in time, within an environmental temperature of -150 °C.

Table 5
Maximum actual displacement presented in [26] and obtained from analytical model at a maximum mechanical loading of 160 N.

Temperature of environment (°C)	100	80	60	40	20	−20	−40	−60	−100	−150
Maximum displacement Experimental (x10^{-3} m)	0.7	0.5	0.45	0.45	0.4	0.3	0.3	0.25	0.25	0.2
Maximum displacement Analytical (x10^{-3} m)	0.3	0.15	0.1	0.08	0.06	0.053	0.05	0.045	0.04	0.03

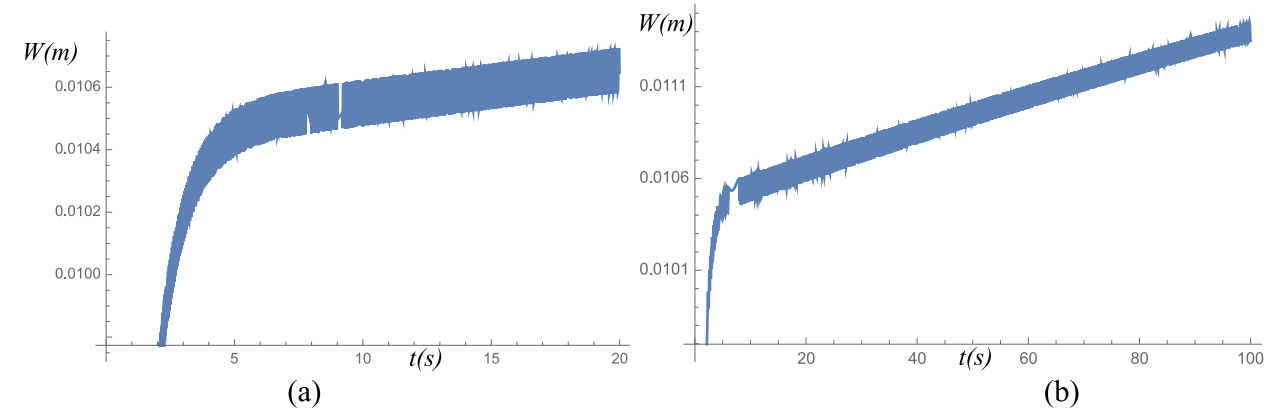

Fig. 12. Displacement response for a larger panel 0.8x0.8 m when subjected to increasing mechanical loading up to 160 N within an environment of 100 °C.

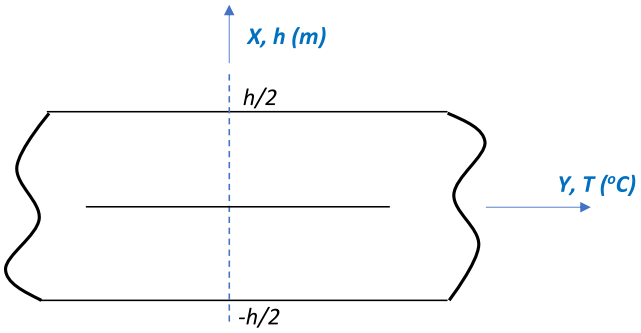

Fig. 13. Representation of the panel for interpretation of temperature distribution across the thickness in Figs. 14-16.

pointed out there that some works have looked at the problem of displacements and stresses in laminated structures under thermal bending. These have assumed a linear temperature profile through the thickness direction for both laminated plates and multilayered composite shells, as well as for circular plates and cylindrical shells. In these models the assumption has been that the temperature profile through the thickness is of linear and constant nature. This assumption could not be valid for anisotropic structures where the thickness temperature profile is never linear. Therefore, even if the structural model is accurate, the final solution could be in error due to the incorrectly assumed profile of the temperature distribution along the thickness. In [9,10] it has been shown that dependent on how the displacement and/or stress field are presented in the normal direction, mathematical models for thermal analysis of composite laminates can be derived using the three-dimensional theory of elasticity, Equivalent Single Layer theories (ESL), Layer Wise theories (LW) or zig-zag theories, and more recently by means of Carrera's Unified Formulation (CUF). To reduce the computational cost of three-dimensional theories and also maintain acceptable accuracy, several solutions for the thermal problems in composites have been proposed using the ESLs. These are the Classical Laminated Plate Theory (CLPT), First-order Shear Deformation Theory (FSDT) and Higher-order Shear Deformation Theory (HSDT). It has been highlighted in [8] that the literature so far only contains a relatively small amount of work devoted to the coupled thermo-mechanical analysis of structures, in the form of both thermoelastic and thermo-plastic analyses. There also have been some works comparing coupled and uncoupled analysis, the accuracy and efficiency of the coupled

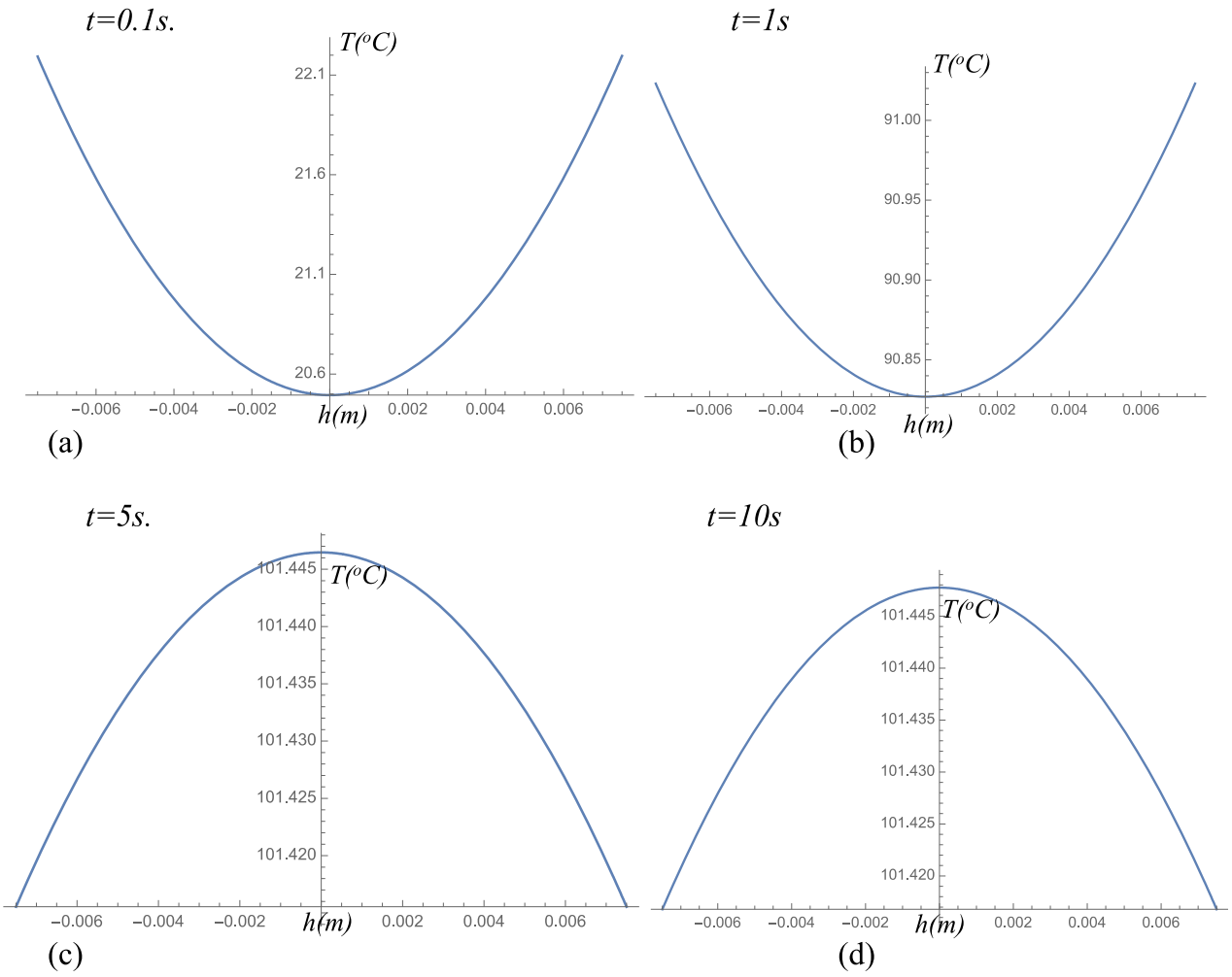

Fig. 14. Temperature distribution across the thickness of the panel (x coordinate) when the panel is under dynamic mechanical loading and in an environmental soak temperature of 100 °C, presented for different instants in time.

theory [11], and the extension of a higher-order zig-zag plate theory [12] for prediction of the fully coupled mechanical, thermal, and electric behaviour. Partially coupled models are commonly derived that neglect the interactions between temperature effects and mechanical deformations, and instead assume *a priori* the distribution of temperature along the thickness, or obtain it from the heat conduction equation and then they solve the mechanical equations with known temperature gradient terms. In contrast, fully coupled thermoelastic models take into account explicitly the interaction between temperature effects and mechanical deformations, because of the presence of coupling displacement and temperature terms in the thermal and mechanical equations, respectively. Furthermore, if the temperature varies in time we deal with two coupled processes, the *reversible elastic process* and the *irreversible thermodynamic process,* due to a spontaneous and hence irreversible process of heat transfer by means of heat conduction). This means that fully coupled approaches are the most appropriate for model development to investigate the influence of the thermal loading on the global thermomechanical behaviour of the structure.

From the foregoing discussion it can be seen that in order to consider thermoelasticity reasonably properly it is necessary to accept that deformation of a body leads to temperature changes, and conversely, and the internal energy of the body depends on both the temperature and the deformation. Therefore, for increased accuracy the problem has to be treated as a *coupled* process.

In this paper, to try to reduce the computational cost, it was decided to implement the Third order theory with Thermomechanical Coupling (TTC) approach described in [13]. This approach is a third order theory with thermomechanical coupling and demonstrated in [13] as giving results as accurate as those obtained from using CUF, which is a fully coupled approach using a fourth order expansion of the configuration variables. The underlying theory is extensive and covers a wide range of approaches and cases, which means that we are able to introduce the necessary simplifications to incorporate appropriate boundary and initial conditions.

It should also be mentioned that in recent years honeycomb panels have become more and more widely used within the aerospace industry [4,14,15,16] due to their structural efficiency, and because they demonstrate a generally high strength to weight ratio. This type of design consists of two thin parallel face sheets separated typically by a cellular foil core that transmits transverse shear and via skin separation has a naturally high cross-sectional second moment of area. The core can be composed of different types of material, but the most frequently used one is a hexagonal honeycomb made from sheets of aluminium foil (Fig. 1). Despite their many benefits sandwich panels do have a number of structural limitations. They are known to have poor resistance to impact loads, particularly when combined with thermal loading, due to the risk of debonding between the sandwich core and the outer faces under these conditions.

In this paper we consider a typical aerospace aluminium honeycomb sandwich panel, this being a generally common form of structural material encountered across the aerospace industry (Fig. 1).

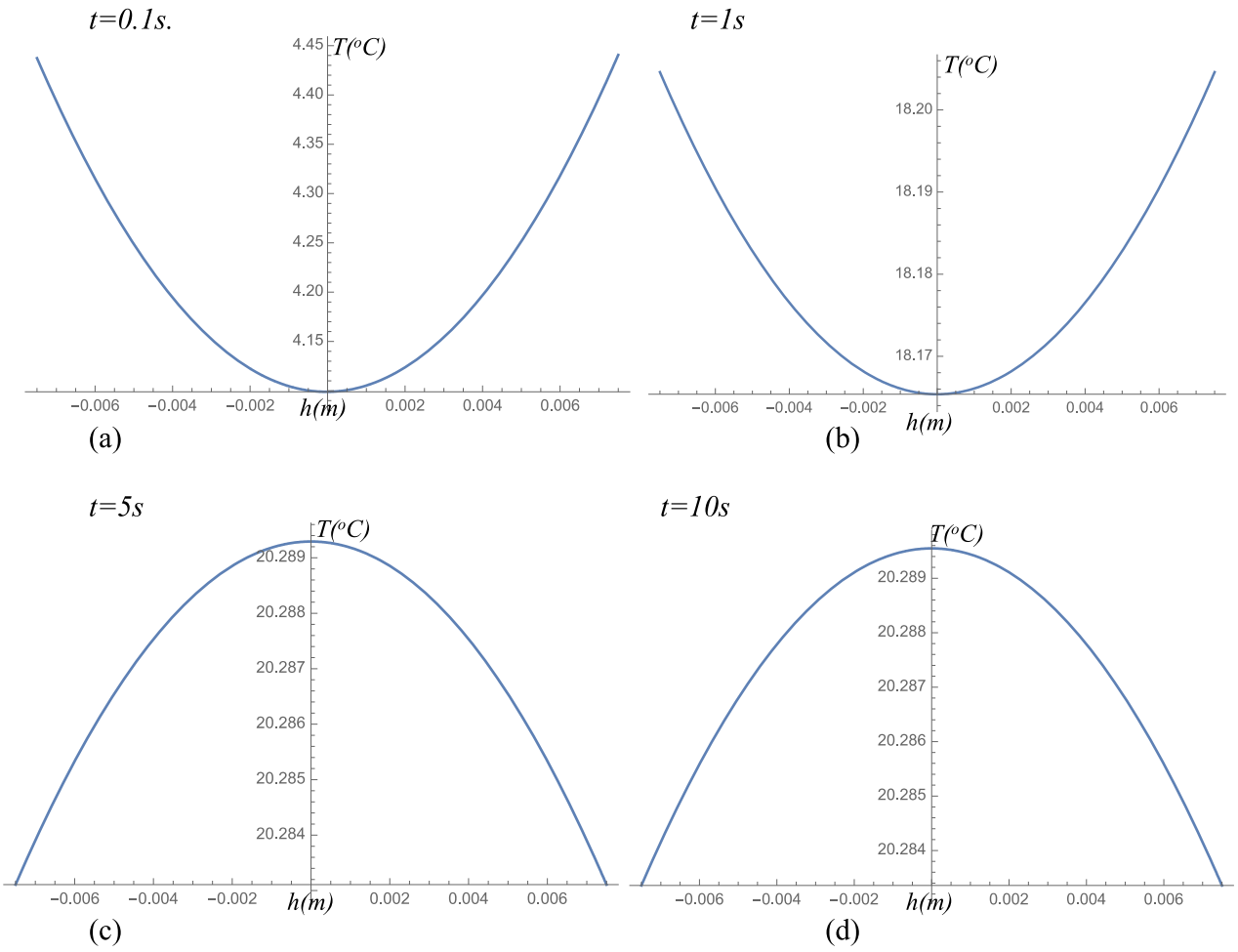

Fig. 15. Temperature distribution across the thickness of the panel (x coordinate) when the panel is under dynamic mechanical loading and in an environmental soak temperature of 20 °C, presented for different instants in time.

2. Aluminium alloy composite panel

The type of sandwich panel considered here for modelling is an offcut of a typical industrial aerospace panel, and is composed of two grades of aluminium alloy Al-2024 and Al-5056 and was identical to the material investigated experimentally in [17]. For the outer faces of thickness $0.38{\cdot}10^{-3}$ m, an Al-2024 alloy is used, whilst an Al-5056 alloy foil is used to form the hexagonal honeycomb core. This core is of depth 14.24 $x10^{-3}$ m and comprises a foil of thickness 0.0254 $x10^{-3}$m. The mechanical and thermal properties of these materials for the offcut supplied, excluding the adhesive, were reconstructed from confidential industrial correspondence, and Hexcel standards for 3/16″ honeycomb [18] and [19]. These properties are summarised in Tables 1 and 2, noting that the data in Table 1 does not contain explicit information on the thin film adhesive bonding of the core to the skin because this is not included in the model as applied here. It should be noted that the density of the Al-5056 core is much lower than that of the Al-2024 skins because it is an average figure covering the material itself and the volumetrically large voids within the honeycomb.

Despite the fact that finite element analysis is widely used for thermo-mechanical analysis, there is a significant industrial need for modelling that can avoid major re-definitions of statically and dynamically correlated spacecraft system level models. Ideal modelling should be capable of 'communication' between the mechanical and thermal aspects of the problem in order to predict the behaviour of the panel accurately in time. Such a facility would provide further insight into areas such as the structural reliability of the system, the dynamic changes in the structural properties due to thermo-mechanical loadings, and potential resonances arising from thermal loading and structural changes within the panel.

It is also desirable that this model remains conceptually straightforward in use and is able to accommodate different mechanical and thermal boundary conditions as well as dynamic mechanical and thermal loading, in order to simulate properly the behaviour of different structural elements. Clearly, the middle core will generally behave differently from the top and bottom plies, both mechanically and thermally. It is hypothesised that the middle core will experience nonlinear non-uniform deformation due to the long-lasting heating effects that it experiences from the top and bottom layers. This means that the model needs to accommodate dynamically varying thermal properties.

To keep the model tractable it has been decided to implement a partially coupled TTC model. Although TTC in [13,21] is partially coupled it still demonstrates very high accuracy when compared with the fully coupled CUF model [8,20]. The TTC model consists of well-developed mechanical and thermal parts connected through additional coupling terms, these being temperature and time dependent in the mechanical part, and displacement and time dependent in the thermal part, respectively.

3. A model for the mechanical behaviour of the panel

The mechanical equations of motion are based on the Reddy plate theory [13] and [22], and an adaptation of this follows on directly, noting that it is assumed that deflection due to shear is negligible with

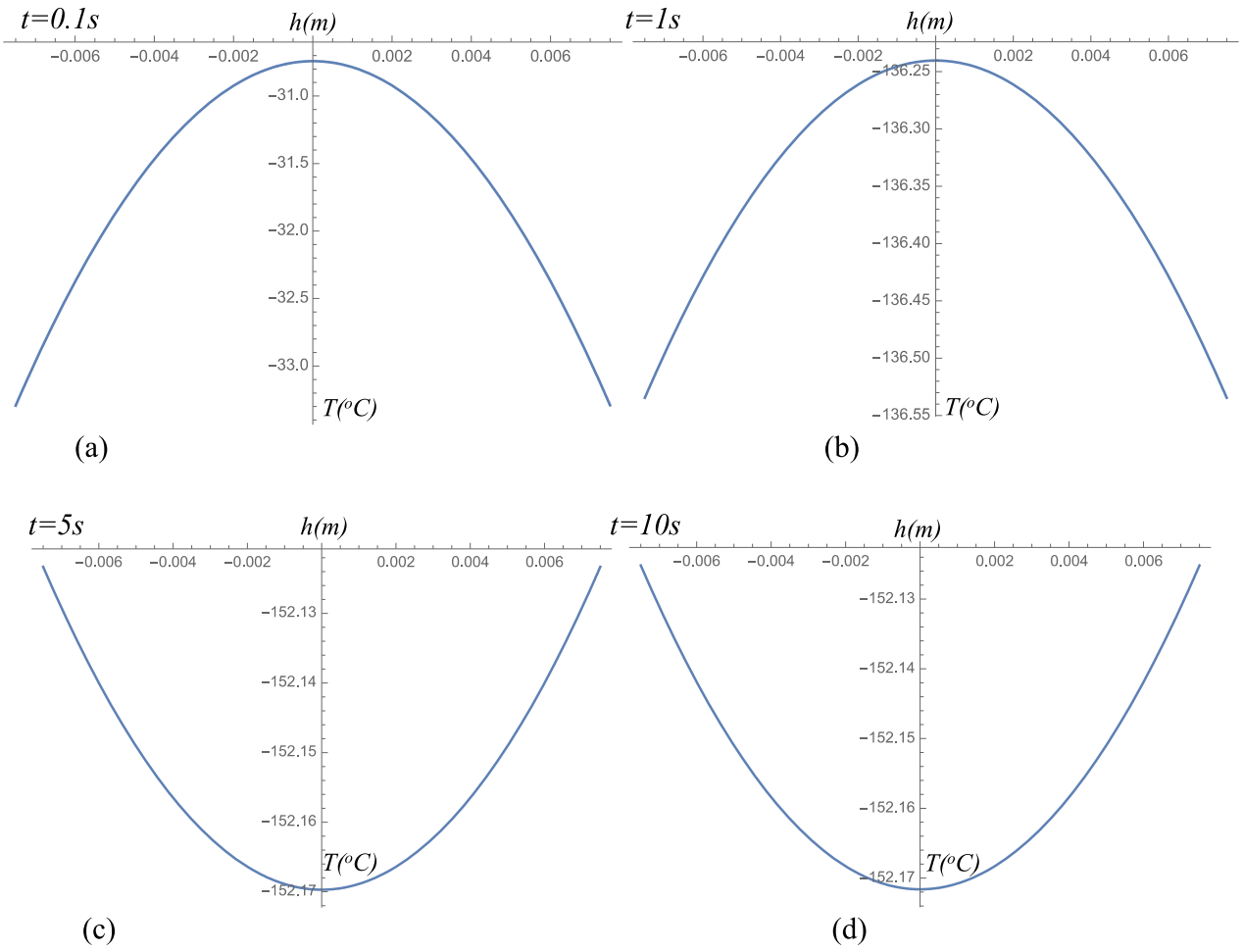

Fig. 16. Temperature distribution across the thickness of the panel (x coordinate) when the panel is under dynamic mechanical loading and in an environmental soak temperature of −150 °C, presented for different instants in time.

respect to flexure between the layers, and so the basis for the model has been reduced to the interpretation given by [22],

$$N_{11,x} + N_{12,y} = 0$$

$$N_{12,x} + N_{22,y} = 0$$

$$M_{11,xx} + 2M_{12,xy} + M_{22,yy} + N_{11}w_{,xx} + 2N_{12}w_{,xy} + N_{22}w_{,yy} + q(x,y,t) - p_x w_{,xx} - p_y w_{,yy}$$

$$= \rho h w_{,tt} + \delta w_{,t}$$

where

$$\begin{Bmatrix} N_{11} \\ N_{22} \\ N_{12} \end{Bmatrix} = \int_{-h/2}^{h/2} \begin{Bmatrix} \sigma_{11} \\ \sigma_{22} \\ \sigma_{12} \end{Bmatrix} dz; \begin{Bmatrix} M_{11} \\ M_{22} \\ M_{12} \end{Bmatrix} = \int_{-h/2}^{h/2} z \begin{Bmatrix} \sigma_{11} \\ \sigma_{22} \\ \sigma_{12} \end{Bmatrix} dz;$$

and where N_{ij} are membrane forces, M_{ij} are bending moments, p_x and p_y are forces applied along the x and y coordinate directions respectively, δ is a damping coefficient, $q(x,y,t)$ is a transversely distributed loading, and ρ and h are the density and thickness of the panel.

For a laminated plate with arbitrarily oriented plies, the thermoelastic linear constitutive relations for the kth orthotropic lamina in the principal material coordinates of the lamina are,

$$\begin{Bmatrix} \sigma_{11} \\ \sigma_{22} \\ \sigma_{12} \end{Bmatrix} = \begin{bmatrix} \overline{Q}_{11} & \overline{Q}_{12} & 0 \\ \overline{Q}_{12} & \overline{Q}_{22} & 0 \\ 0 & 0 & \overline{Q}_{66} \end{bmatrix}^{(k)} \begin{Bmatrix} \varepsilon_{11} \\ \varepsilon_{22} \\ \varepsilon_{12} \end{Bmatrix} - \begin{Bmatrix} \beta_{11} \\ \beta_{22} \\ 0 \end{Bmatrix}^{(k)} T \tag{3}$$

where $\overline{Q}_{ij}^{(k)}$ are the plane stress-reduced elastic stiffnesses, and $\overline{\beta}_{11}^{(k)} = \overline{Q}_{11}^{(k)}\alpha_1 + \overline{Q}_{12}^{(k)}\alpha_2$ and $\overline{\beta}_{22}^{(k)} = \overline{Q}_{12}^{(k)}\alpha_1 + \overline{Q}_{22}^{(k)}\alpha_2$ are the thermoelastic stiffnesses, with α_1 and α_2 being the coefficients of thermal expansion in the x and y directions.

The relationships between strains and displacements are given by the following [13],

$$\varepsilon_{11}^{(0)} = u_{,x} + \frac{1}{2}w_{,x}^2; \varepsilon_{22}^{(0)} = v_{,y} + \frac{1}{2}w_{,y}^2$$

$$\varepsilon_{12}^{(0)} = u_{,y} + v_{,x} + w_{,x}w_{,y} \tag{4}$$

$$\varepsilon_{12}^{(3)} = -C_1(2w_{,xy}), \text{ where } C_1 = 4/(3h^2) \tag{5}$$

and $u(x,y,t)$, $v(x,y,t)$, $w(x,y,t)$ are the displacements of a point located on the mid-plane, where the comma is used in the conventional way to denote the derivative compactly with respect to the associated independent variables.

The strains in Eq. (4) are related to the three dimensional strains in Eq. (6), as in [13], neglecting the rotations of the transverse normal around the x- and y- axes,

$$\varepsilon_{11} = \varepsilon_{11}^{(0)}; \varepsilon_{22} = \varepsilon_{22}^{(0)}; \varepsilon_{12} = \varepsilon_{12}^{(0)} + z^3\varepsilon_{12}^{(3)} \tag{6}$$

In Eqs.(4)-(6), $\varepsilon_{ij}^{(0)}$ are the von Karman nonlinear membrane strains, $\varepsilon_{ij}^{(3)}$ are the Reddy higher order bending strains. The transverse shearing strains are neglected.

Following [13] we also assume that the temperature varies according to a cubic law,

$$T = T_0 + zT_1 + z^2T_2 + z^3T_3 \tag{7}$$

where $T(x,y,z,t)$ is the three dimensional temperature variable, while $T_0(x,y,t), T_1(x,y,t), T_2(x,y,t), T_3(x,y,t)$ are the hitherto unknown components of the temperature of the two dimensional model, and cover the full profile up to a cubic distribution.

The components T_2 and T_3 can be expressed in terms of T_0 and T_1 by imposing a variable combination of the following thermal boundary condition, in this case a +/- distribution of the free heat exchange on the upper and lower surfaces of the plate [20,23],

$$q_3|_{z=\pm h/2} = \pm H\left[T_\infty - (T)_{\pm h/2}\right] \text{ (for free heat exchange)} \tag{8}$$

where q_3 is the heat flow in the z direction, H is the boundary conductance, and T_∞ is a constant difference between the absolute temperature of the surrounding medium and the reference temperature,

$$T = f_a(z)T_0 + f_b(z)T_1 + f_c(z) \tag{9}$$

where

$$f_a(z) = (r_1 + r_2z + r_3z^2 + r_4z^3)$$

$$f_b(z) = \left(r_5 + r_6z + r_7z^2 + r_8z^3\right)$$

$$f_c(z) = (r_9 + r_{10}z + r_{11}z^2 + r_{12}z^3) \tag{10}$$

and where the r_i are defined by the imposed boundary conditions. For a free heat exchange thermal boundary condition the r_i are introduced as given in [13,23],

$$r_1 = r_6 = 1; r_3 = -\frac{4H}{h\left(hH + 4\lambda_{33}^{(1)}\right)}; r_8 = -\frac{4(hH + 2\lambda_{33}^{(1)})}{h^2(hH + 6\lambda_{33}^{(1)})}$$

$$r_{11} = \frac{4HT_\infty}{h\left(hH + 4\lambda_{33}^{(1)}\right)}; r_2 = r_4 = r_5 = r_7 = r_9 = r_{10} = r_{12} = 0$$

where the $\lambda_{ij}^{(k)}$ are the thermal conductivities of the kth laminate.

4. A model for the thermal behaviour of the panel

The thermal balance equations are introduced for the case of non-stationary conduction and thermoelastic coupling, as in [13],

$$q_{1,x} + q_{2,y} + q_{3,z} - b_{,t} - a_{,t} + E = 0 \tag{11}$$

where the $q_i(x,y,z,t)$ represents the three dimensional heat flow along the x,y,z directions, $b(x,y,z,t)$ is the three dimensional internal energy due to non-stationary conduction, $a(x,y,z,t)$ is the three dimensional interaction energy due to the thermoelastic coupling, and $E(x,y,z,t)$ is the three dimensional source energy. The two-dimensional balance consists of two equations obtained from Eq. (11), [13,21],

$$q_{1,x}^{(0)} + q_{2,y}^{(0)} - b_{,t}^{(0)} - a_{,t}^{(0)} + Q^{(0)} = 0$$

$$q_{1,x}^{(1)} + q_{2,y}^{(1)} - b_{,t}^{(1)} - a_{,t}^{(1)} + Q^{(1)} = 0 \tag{12}$$

where the following two dimensional quantities are defined as

$$\begin{Bmatrix} q_1^{(0)} \\ q_2^{(0)} \end{Bmatrix} = \int_{-h/2}^{h/2} \begin{Bmatrix} q_1 \\ q_2 \end{Bmatrix} dz; b^{(0)} = \int_{-h/2}^{h/2} bdz; a^{(0)} = \int_{-h/2}^{h/2} adz$$

$$\begin{Bmatrix} q_1^{(1)} \\ q_2^{(1)} \end{Bmatrix} = \int_{-h/2}^{h/2} z\begin{Bmatrix} q_1 \\ q_2 \end{Bmatrix} dz; b^{(1)} = \int_{-h/2}^{h/2} bzdz; a^{(1)} = \int_{-h/2}^{h/2} azdz$$

$$Q^{(0)} = \int_{-h/2}^{h/2} q_{3,z}dz; Q^{(1)} = \int_{-h/2}^{h/2} q_{3,z}zdz \tag{13}$$

The source energy $E(x,y,z,t)$ is neglected due to the absence of chemical reactions, nuclear fission effects or inputs due to electric currents. The heat flow definition is based on the Fourier law for the kth orthotropic lamina and expressed in the principal material coordinates of a lamina as follows,

$$\begin{Bmatrix} q_1^{(0)} \\ q_2^{(0)} \end{Bmatrix} = \sum_{k=1}^{N} \int_{z_k}^{z_{k+1}} \begin{bmatrix} \lambda_{11}^{(k)} & \lambda_{12}^{(k)} \\ \lambda_{12}^{(k)} & \lambda_{22}^{(k)} \end{bmatrix} \left(\begin{bmatrix} f_a(z) & 0 \\ 0 & f_a(z) \end{bmatrix} \begin{Bmatrix} g_1^{(0)} \\ g_2^{(0)} \end{Bmatrix} + \right.$$

$$\left. + \begin{bmatrix} f_b(z) & 0 \\ 0 & f_b(z) \end{bmatrix} \begin{Bmatrix} g_1^{(1)} \\ g_2^{(1)} \end{Bmatrix} \right) dz$$

$$\begin{Bmatrix} q_1^{(1)} \\ q_2^{(1)} \end{Bmatrix} = \sum_{k=1}^{N} \int_{z_k}^{z_{k+1}} \begin{bmatrix} \lambda_{11}^{(k)} & \lambda_{12}^{(k)} \\ \lambda_{12}^{(k)} & \lambda_{22}^{(k)} \end{bmatrix} \left(\begin{bmatrix} f_a(z) & 0 \\ 0 & f_a(z) \end{bmatrix} \begin{Bmatrix} g_1^{(0)} \\ g_2^{(0)} \end{Bmatrix} + \right.$$

$$\left. + \begin{bmatrix} f_b(z) & 0 \\ 0 & f_b(z) \end{bmatrix} \begin{Bmatrix} g_1^{(1)} \\ g_2^{(1)} \end{Bmatrix} \right) zdz \tag{14}$$

where the $\lambda_{ij}^{(k)}$ are the thermal conductivities of the kth laminate, and thermal gradients $g_1^{(0)} = T_{0,x}, g_1^{(1)} = T_{1,x}, g_2^{(0)} = T_{0,y}, g_2^{(1)} = T_{1,y}$ as defined in [13].

The internal energy for the kth lamina is defined in terms of temperature,

$$b^{(k)} = C^{(k)}T = \rho^{(k)}c_v^{(k)} \tag{15}$$

where $C^{(k)}$ is the thermal capacity of the kth lamina, the function of mass density is $\rho^{(k)}$ and the specific heat at constant strain is given by $c_v^{(k)}$.

The components of internal energy can then be re-written, taking into account Eqs. (9)-(10), (15), as,

$$b^{(0)} = \int_{-h/2}^{h/2} bdz = \sum_{k=1}^{N} \int_{z_k}^{z_{k+1}} b^{(k)}dz$$
$$= \sum_{k=1}^{N} \int_{z_k}^{z_{k+1}} C^{(k)}[f_a(z)T_0 + f_b(z)T_1 + f_c(z)]dz \tag{16}$$

$$b^{(1)} = \int_{-h/2}^{h/2} bdz = \sum_{k=1}^{N} \int_{z_k}^{z_{k+1}} b^{(k)}dz$$
$$= \sum_{k=1}^{N} \int_{z_k}^{z_{k+1}} C^{(k)}[f_a(z)T_0 + f_b(z)T_1 + f_c(z)]zdz \tag{17}$$

The interaction energy for the kth orthotropic lamina is expressed in terms of strain within the three dimensional thermoelastic theory, with the assumption that $\varepsilon_{zz} = \varepsilon_{33} = 0$,

$$a^{(0)} = \int_{-h/2}^{h/2} adz = \sum_{k=1}^{N} \int_{z_k}^{z_{k+1}} a^{(k)}dz =$$

$$= T_{ref} \sum_{k=1}^{N} \int_{z_k}^{z_{k+1}} \left[\beta_{11}^{(k)}\left(\varepsilon_{11}^{(0)} + z\varepsilon_{11}^{(1)} + z^3\varepsilon_{11}^{(3)}\right) + \beta_{22}^{(k)}\left(\varepsilon_{22}^{(0)} + z\varepsilon_{22}^{(1)} + z^3\varepsilon_{22}^{(3)}\right) + \right.$$

$$\left. + \beta_{12}^{(k)}\left(\varepsilon_{12}^{(0)} + z\varepsilon_{12}^{(1)} + z^3\varepsilon_{12}^{(3)}\right)\right] dz$$

$$a^{(1)} = \int_{-h/2}^{h/2} a z dz = \sum_{k=1}^{N} \int_{z_k}^{z_{k+1}} a^{(k)} z dz =$$

$$= T_{ref} \sum_{k=1}^{N} \int_{z_k}^{z_{k+1}} \left[\beta_{11}^{(k)} \left(\varepsilon_{11}^{(0)} + z\varepsilon_{11}^{(1)} + z^3 \varepsilon_{11}^{(3)} \right) + \beta_{22}^{(k)} \left(\varepsilon_{22}^{(0)} + z\varepsilon_{22}^{(1)} + z^3 \varepsilon_{22}^{(3)} \right) + \right.$$

$$\left. + \beta_{12}^{(k)} \left(\varepsilon_{12}^{(0)} + z\varepsilon_{12}^{(1)} + z^3 \varepsilon_{12}^{(3)} \right) \right] z dz \tag{18}$$

The energy exchange rates of the out-of-plane heat flow $Q^{(0)}$ and $Q^{(1)}$ due to the heat flow q_3 in the z direction are,

$$Q^{(0)} = \int_{-h/2}^{h/2} q_{3,z} dz = \sum_{k=1}^{N} \int_{z_k}^{z_{k+1}} \lambda_{33}^{(k)} g_{3,z} dz = \sum_{k=1}^{N} \int_{z_k}^{z_{k+1}} \lambda_{33}^{(k)} \left[(f_a(z) T_0 + f_b(z) T_1 + f_c(z))_{,zz} \right] dz$$

$$Q^{(1)} = \int_{-h/2}^{h/2} q_{3,z} z dz = \sum_{k=1}^{N} \int_{z_k}^{z_{k+1}} \lambda_{33}^{(k)} g_{3,z} z dz = \sum_{k=1}^{N} \int_{z_k}^{z_{k+1}} \lambda_{33}^{(k)} \left[(f_a(z) T_0 + f_b(z) T_1 + f_c(z))_{,zz} \right] dz \tag{19}$$

A procedure specifically for computing the solutions to the principal equations (1) and (12), and invoking all the parameters that follow, defined with respect to specified boundary and initial conditions, has been coded in the *Mathematica*™ programming language.

Having derived the necessary components of the thermal and mechanical equations it is then possible to obtain the system of equations. Since we are interested in the temperature and displacement distribution in the *z*-direction for the structure when it is subjected to combined mechanical and thermal loading, the system can be reduced to the following three equations to find the displacement $W(t)$, membrane temperature $T_0(t)$ and bending temperature $T_1(t)$ as defined in [21,24], and then to identify $T(t)$ in Eq.(9):

$$C_1 \ddot{W}(t) + C_2 \dot{W}(t) + \left[C_3 + C_4 p_x(t) + C_5 p_y(t) + C_6 T_0(t) + C_7 T_\infty(t) \right] W(t)$$
$$+ C_8 W^3(t)$$
$$+ C_9 T_1(t) + q(t) = 0$$

$$C_{10} \dot{T}_0(t) + C_{11} T_0(t) + C_{12} T_\infty(t) + C_{13} \dot{W}(t) W(t) = 0$$

$$C_{16} \dot{T}_1(t) + C_{17} T_1(t) + C_{18} T_\infty(t) + C_{19} \dot{W}(t) = 0 \tag{20}$$

It has to be pointed out that in reference [13] this form of system of equations was solved analytically obtaining a general solution using features within a *Mathematica*™ code. However, this was done by eliminating the nonlinear terms and for static values of the mechanical and thermal loading, thus,

$$C_1 \ddot{W}(t) + C_3 W(t) + C_9 T_1(t) = 0$$

$$C_{10} \dot{T}_0(t) + C_{11} T_0(t) = 0$$

$$C_{16} \dot{T}_1(t) + C_{17} T_1(t) + C_{19} \dot{W}(t) = 0 \tag{21}$$

Here our overall aim has been to look for a solution for the system in its generalised form, as stated in full in Eq. (20). The implications of the simplification in Eq. (21) were discussed in [25].

5. Numerical experiment

A numerical study is presented for the solutions obtained for the system (20) with full nonlinear coupling terms, and by exploiting the powerful numerical functions within NDSolve. The loading is considered as a combined thermo-mechanical load consisting of a constant thermal component and a dynamic mechanical component.

The plate-like panel under consideration is of the dimensions provided in Table 3, in line with the geometry of the industrial specimen used experimentally in [17]. These properties, as well as loading conditions and boundary and initial conditions, are considered for verification of the performance of the model against the experimental results presented in [17].

The panel was considered to be simply supported and was analysed under dynamic mechanical loading increasing up to 160 N while being positioned within an environmental chamber exhibiting thermal loading in the form of a variety of thermal environments simulating the experimental configuration discussed in [17]. Within the analytical model thermal loading was applied by means of imposing different environmental temperatures in order to represent free heat exchange conditions similar to those of the experiment in [17], and mechanical loading was taken as a dynamically increasing normal force governed by $q(t) = 10*t$ to simulate a ramped increase up to 160 N after 16 s has elapsed, and this is applied centrally to the top-face sheet.

It should be pointed out that in the experiment [17] an initial displacement was introduced to more clearly portray the gradual displacement that emerged naturally within the experiment, therefore in order to calculate the actual displacement from the graphs presented in [26] the initial displacement has to be deducted.

Based on the results presented graphically in [26] the maximum value of the actual displacement is summarised in Table 4. These outputs from the experiment will be used for verification of the model discussed in this paper.

5.1. Displacement distribution in response to the dynamic mechanical loading and variable environmental temperature

When elevated temperature conditions apply at the outer faces of the sandwich panel, representing the free heat exchange condition, these

faces will heat up first of all, with the heat then distributing from the outer faces inwards towards the centre of the core. To understand the process of the displacement due to the heating-up process, as well as the characteristics of the thermal gradient along the thickness, a constant environmental surround temperature of 100 °C, 80 °C, 60 °C, 40 °C and ambient as 20 °C were applied with the ambient reference temperature set to 20 °C, and a solution for the system of Eq. (20) was obtained using the NDSolve function in *Mathematica*™ and presented in Figs. 2-6 corresponding to the temperature of the environment.

Figs. 2-6 (a) demonstrate the maximum value of the displacement after 16 s when it has reached 160 N according to the loading being represented by $q(t) = 10*t$, as corresponding with the experimental study in [17]. As can be seen in Figs. 2-6 (a) there is evidence of an increasing trend in the maximum displacement value, where it is seen to be increasing with the elevating temperature of the environment. This confirms the pattern of behaviour demonstrated in [17] and is summarised in Table 4. It can be justified by the presence of a softening effect of the material within hot environments. This trend becomes even more evident with time, as can be observed in Figs. 2-6 (b).

In Figs. 2-6 we can also see clearly the reflection of the dynamically increasing mechanical loading in an almost linear increasing behaviour of the displacement response. This accords with practical expectations for a plate under this form of loading, as well as with the results for loading up 160 N from the experiment [17].

The principal features of the displacement responses are the transient over time and the largely symmetrical peak to peak amplitudes. It is also important to note that the peak-to-peak transient disturbance increases with the harshness of the environmental temperature, and this confirms the coupling between the environmental heat and the mechanical deformation, and the fact that harsh environments bring in a destabilising effect into the panel's response when undergoing mechanical loading.

To understand the process of the displacement distribution due to the cooler or even extreme environmental conditions a constant environmental surround temperature of −20 °C, −40 °C, −60 °C, −100 °C and −150 °C was applied. A solution for the system of Eq. (20) was again obtained using the NDSolve function in *Mathematica*™ and presented in Figs. 7-11 corresponding to the environmental temperature.

In Table 5 an analysis of the response of the panel to the same increasing mechanical loading $q(t) = 10*t$ but for a colder environment going down to the harsh extreme of −150 °C (Figs. 7-11), confirms the trend demonstrated in [17] which is also summarised in Table 4. The maximum value of the displacement is reached at 16 s and corresponds to 160 N and is decreasing with decreasing environmental temperature (Figs. 7-11 (a)) and this can again be justified by a hardening effect of the material within the colder environment. This trend becomes even more evident at times beyond 16 s, as can be observed in Figs. 7-11 (b). This hardening effect in a colder, harsher, environment also impacts on the transient response. The symmetrical peak to peak amplitude response of displacement clearly decreases, demonstrating stiffer structural properties. However, this 'suppression' of the amplitude might be characterised by a higher frequency response. This confirms the coupling between environmental temperature and mechanical deformation, and the fact that a colder environment is still characterised by a destabilising effect into the panel's response when undergoing mechanical loading.

In Figs. 7-11 we can clearly see again the reflection of the dynamically increasing mechanical loading in an almost linearly increasing behaviour of the displacement response.

It has to be pointed out that the disparity in the results in Table 5 occurs due to the possible inconsistency in material properties, noting that these properties were not known exactly *a priori* for the industrial specimen but were reconstructed from different resources and standards, as discussed in Section 2. Some properties required for the analytical model were not available for the sample tested in [17] therefore typical properties for Al-2024 and Al-5056 were assumed for some of the required material parameters.

For verification of the response of the model the case of a larger plate of dimensions 0.8 × 0.8 m, otherwise with the same properties and under the same mechanical loading in an environment of 100 °C, was considered in Fig. 12.

Comparing the response in Fig. 12 with the results presented in Fig. 2, the panel under consideration with the same thickness but larger length and width dimensions, responds with a larger displacement as expected for a large thin plate.

5.2. Temperature distribution along the thickness of the panel in response to the dynamic mechanical loading and variable environmental temperature

When elevated temperature conditions apply at the outer faces of the sandwich panel, representing the free heat exchange condition, these faces will heat up first of all, with the heat then distributing from the outer faces inwards towards the centre of the core. However, because of differences in the material of the skins and the honeycomb core, it is reasonable to predict a nonlinear temperature distribution along the thickness of the panel. This effect is very difficult to explore experimentally, especially if the panel is relatively thin. But the model applied in this paper allows us to predict the dynamic distribution of the heat along the thickness of the panel.

To understand the process of heating up or cooling down of the panel in response to the high or low environmental temperature, the following values for the constant environmental surround temperature were taken, 100 °C, 80 °C, 60 °C, 40 °C, ambient at 20 °C and then down to −20 °C, −40 °C, −60 °C, −100 °C and −150 °C in line with the investigation of the displacement response considered in 5.1. A solution for the system of Eq. (20) and Eq. (7) was obtained using the NDSolve function in *Mathematica*™ and presented in Figs. 14-16 for environmental temperatures of 100 °C, 20 °C, −150 °C and in Appendix A for 80 °C, 60 °C, 40 °C and then −20 °C, −40 °C, −60 °C, −100 °C.

It should be noted that the thickness of the panel in Figs. 14-16 is along the X coordinate and the temperature readings are along the Y coordinate, as shown schematically in Fig. 13.

By fixing the time steps and observing the progression of the temperature distribution through the plate we see the main stages of the temperature stabilisation process, noting that these are also evident in [13]. In brief, this amounts to the following. By applying heat to the plate through an elevated environmental soak temperature the temperature distribution through the thickness is as shown in Fig. 14(a), with the temperature of the honeycomb core being close to the top skin temperature but slightly cooler by 1.8 °C , and after 1 *s* (Fig. 14(b)) this stabilises and settles within a small difference of 0.2 °C between that of the skin temperature and the honeycomb core. The process of equilibrating temperature due to the plate heating-up progresses further with time and after 5 *s* an equilibrium temperature is reached and the profile thereafter remains constant in time exhibiting a small difference in

temperature between the core and the skins of about 0.03 °C (Fig. 14(c-d).

On analysing the history of the thermal outputs over time for other environments in Figs. 15, 16 and in Appendix A, it is evident that the plate is undergoing a similar process of stabilisation, and reaches the equilibrium state with a small residual disparity in temperature between the skins and core.

From the parabolic output in Fig. 14 it is also obvious that at the start of the heating-up process (time step t = 0.1 s), when the heat is only just starting to distribute through the thickness of the panel, the temperature in the middle is lower than in the skins. However, as the heating-up process progresses, the core, made of thinner honeycomb aluminium, tends to heat up slightly further demonstrating a higher temperature reading around 0.03 °C than that of the skins. A similar flip in the behaviour can be observed for the cooling process shown in Fig. 16, with around 0.04 °C difference between the skins and the core temperature. These internal transformations due to the heating-up or cooling-down process could be the key to an explanation for the transient response demonstrated in the displacement response which is clearly driven by the environmental temperature.

6. Conclusions

1. A new modelling strategy for aluminium honeycomb composite panels widely applied in aerospace structures, has been considered in this paper. The physics of dynamic thermal and mechanical loadings have been integrated into a conceptually straightforward and partially coupled modelling procedure coded in the *Mathematica*™ language which can accommodate different boundary conditions, dynamically varying thermal properties, and dynamic forms of mechanical loading. It has to be pointed out that the generalised model from [13] was applied here only for the free heat-exchange scenario. This is because the work in this paper was intended to verify the model against the experimental work in [17], performed for a industrial panel tested in the laboratory under free heat-exchange in an environmental chamber. Nevertheless, the model can be extended in line with [13] for other thermal conditions by suitably modifying Eqs (8)-(10) in Section 3.
2. The panel presented in the experimental set up in [17] has been considered to verify the analytical model through comparison of the maximum displacement of the panel, as well as the influence of the environmental temperature on the magnitude of displacement induced by a dynamic mechanical loading. The same trend of the higher displacement response in hotter environments and lower displacement response in cooler environments was found, confirming the associated predictions of the analytical model. It was also found that the displacement response was characterised by the transient behaviour, dependent on the environmental temperature, confirming the coupled effects of thermal and mechanical loading.
3. The model was also used to predict the dynamic thermal response of the material within the thickness of the panel, demonstrating a nonlinear temperature distribution profile within the thickness of the panel. It is important to note that this would be very difficult to explore experimentally, especially in practical cases where the panel would be relatively thin. It was also found that during the heating up process the core remains at a lower temperature than the skins were at the beginning of the heating up process. However, there was also evidence of heating up of the core beyond the skin temperature by a very small amount. Although the difference between the temperature of the core and the skins at the end of the transformation was very small, it still gave an indication of some nonlinear transformational phenomena occurring within the thickness of the panel when undergoing mechanical loading within the harsher environments. This of course might be more significant for larger or thicker panels and could be particularly significant for large aerospace structures exposed to harsh thermal cycles.
4. These internal transformations due to the heating-up or cooling-down processes could be the key to the explanation of the transient response demonstrated in the displacement response as driven by the environmental temperature. It is also hypothesised that the frequency of the transient response might be higher due to the amplitude 'suppression' in cooler environments due to the material stiffening effect, which could potentially introduce a parasitic resonance contributing to the problem of de-point of the parent satellite structure. This is still to be investigated in future research.

Funding

The first two authors would like to acknowledge the financial support made available by Airbus Defence & Space Ltd and also the award of funding from the Strathclyde Centre for Doctoral Training. The authors would also like to thank Airbus Defence & Space Ltd for confidential access to data, noting that no disclosure of any such data whatsoever has been made within this paper.

Data availability statement

The raw/processed data required to reproduce these findings cannot be shared at this time due to legal or ethical reasons.

CRediT authorship contribution statement

Olga A. Ganilova: Supervision, Visualization, Writing – review & editing, Writing – original draft, Investigation, Formal analysis, Validation, Software, Methodology, Conceptualization. **Matthew P. Cartmell:** Supervision, Writing – review & editing, Writing – original draft, Investigation, Formal analysis, Conceptualization. **Andrew Kiley:** Funding acquisition, Resources, Conceptualization.

Declaration of Competing Interest

The authors declare that they have no known competing financial interests or personal relationships that could have appeared to influence the work reported in this paper.

Acknowledgements

The first two authors would like to acknowledge the financial support made available by Airbus Defence & Space Ltd and also the award of funding from the Strathclyde Centre for Doctoral Training. The authors would also like to thank Airbus Defence & Space Ltd for confidential access to data, noting that no disclosure of any such data whatsoever has been made within this paper.

Appendix A

See Figs. A1-A7.

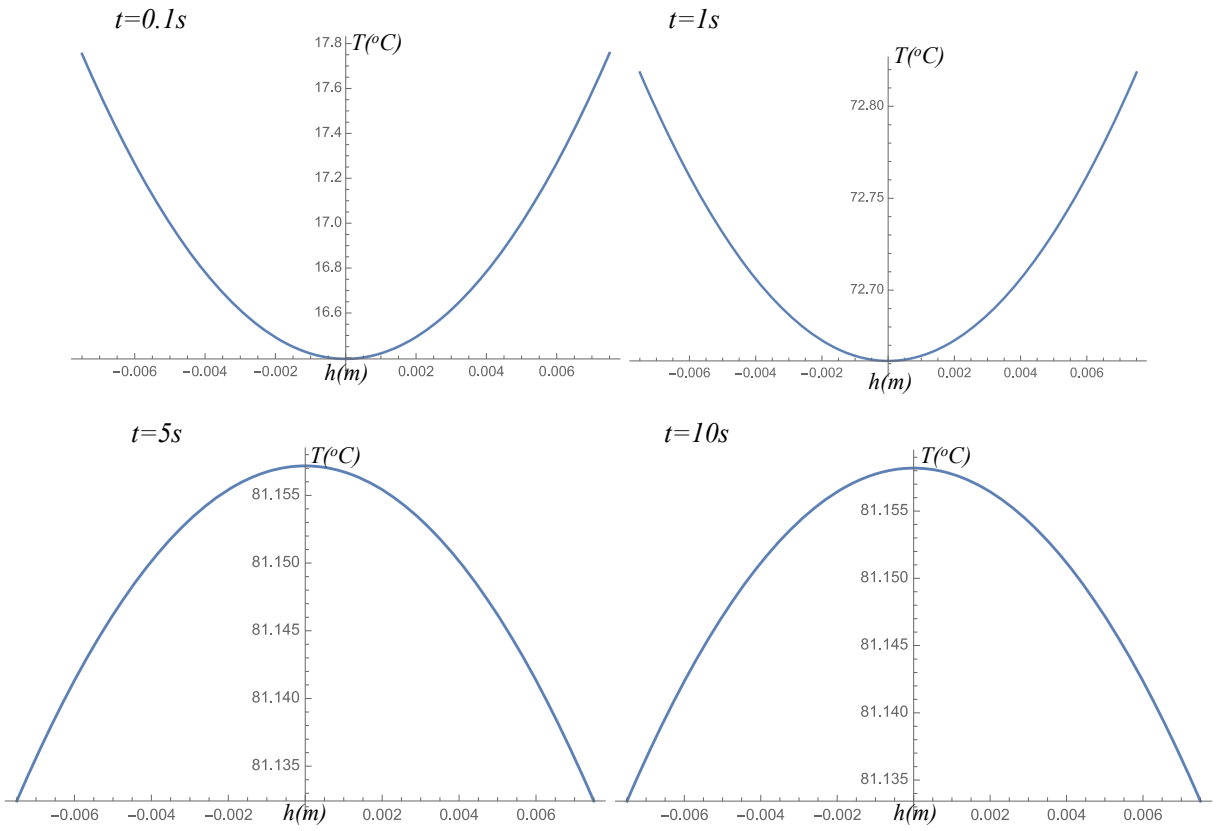

Fig. A1. Temperature distribution across the thickness of the panel (x coordinate) when the panel is under dynamic mechanical loading and in an environmental soak temperature of 80 °C, presented at different instants in time.

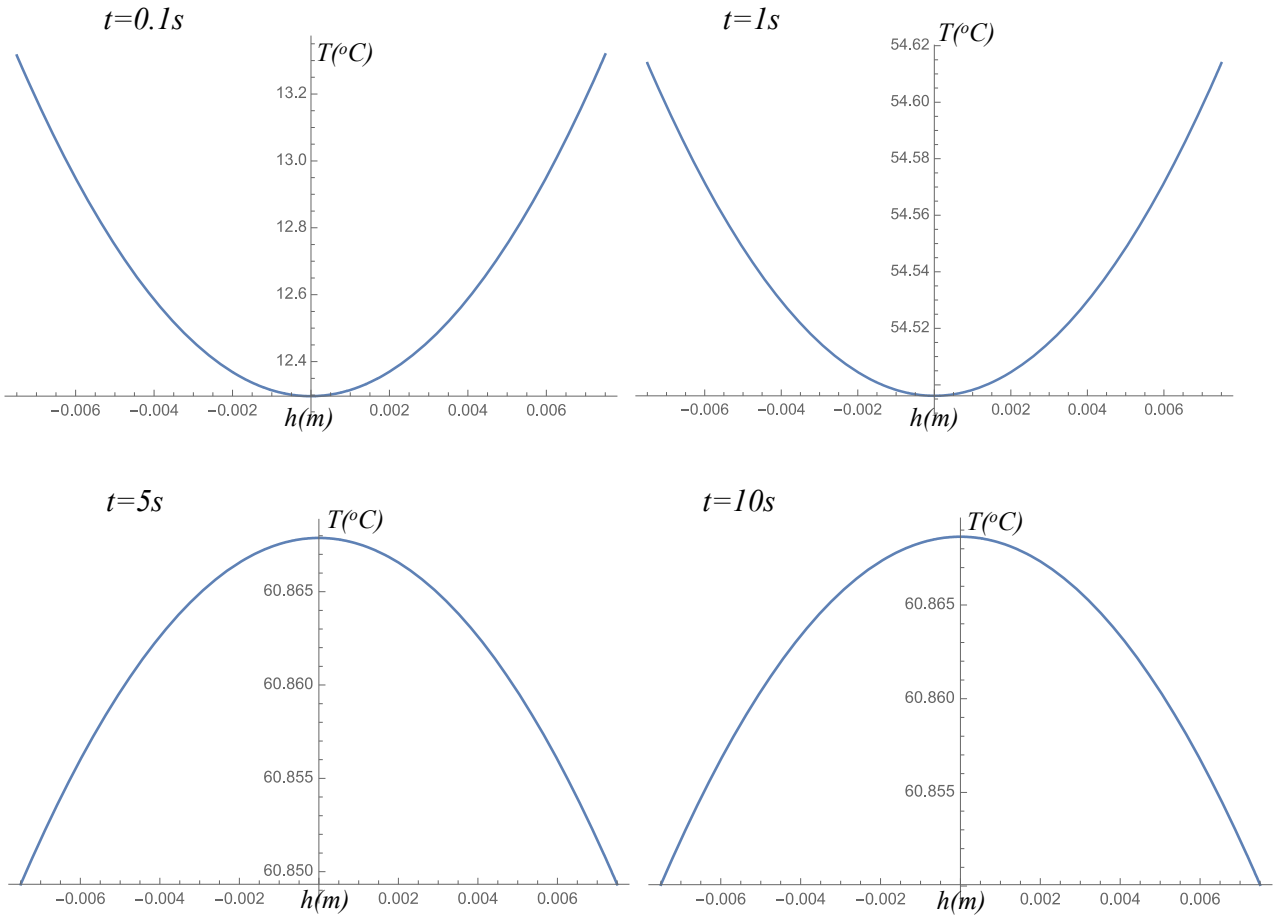

Fig. A2. Temperature distribution across the thickness of the panel (x coordinate) when the panel is under dynamic mechanical loading and in an environmental soak temperature of 60 °C, presented at different instants in time.

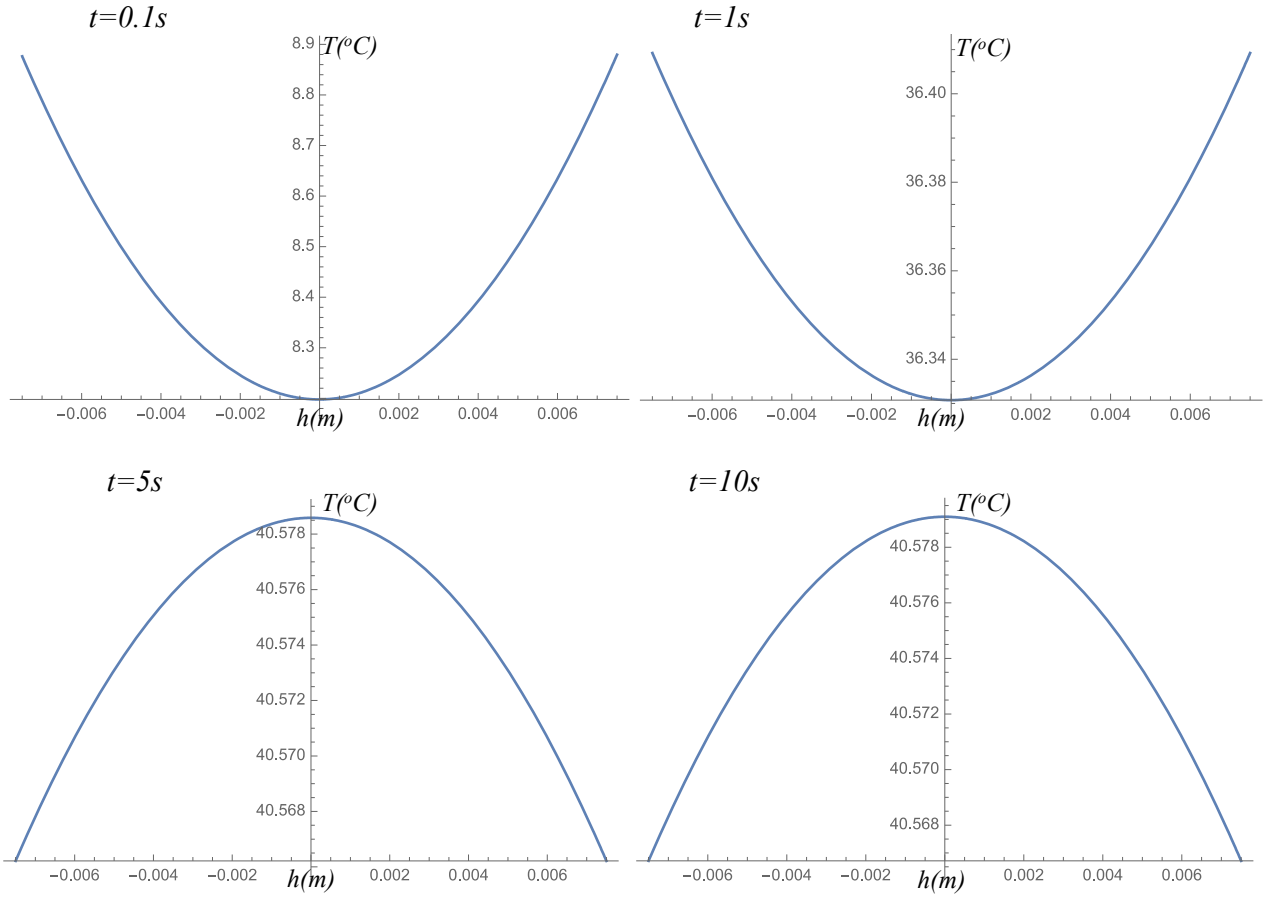

Fig. A3. Temperature distribution across the thickness of the panel (x coordinate) when the panel is under dynamic mechanical loading and in an environmental soak temperature of 40 °C, presented at different instants in time.

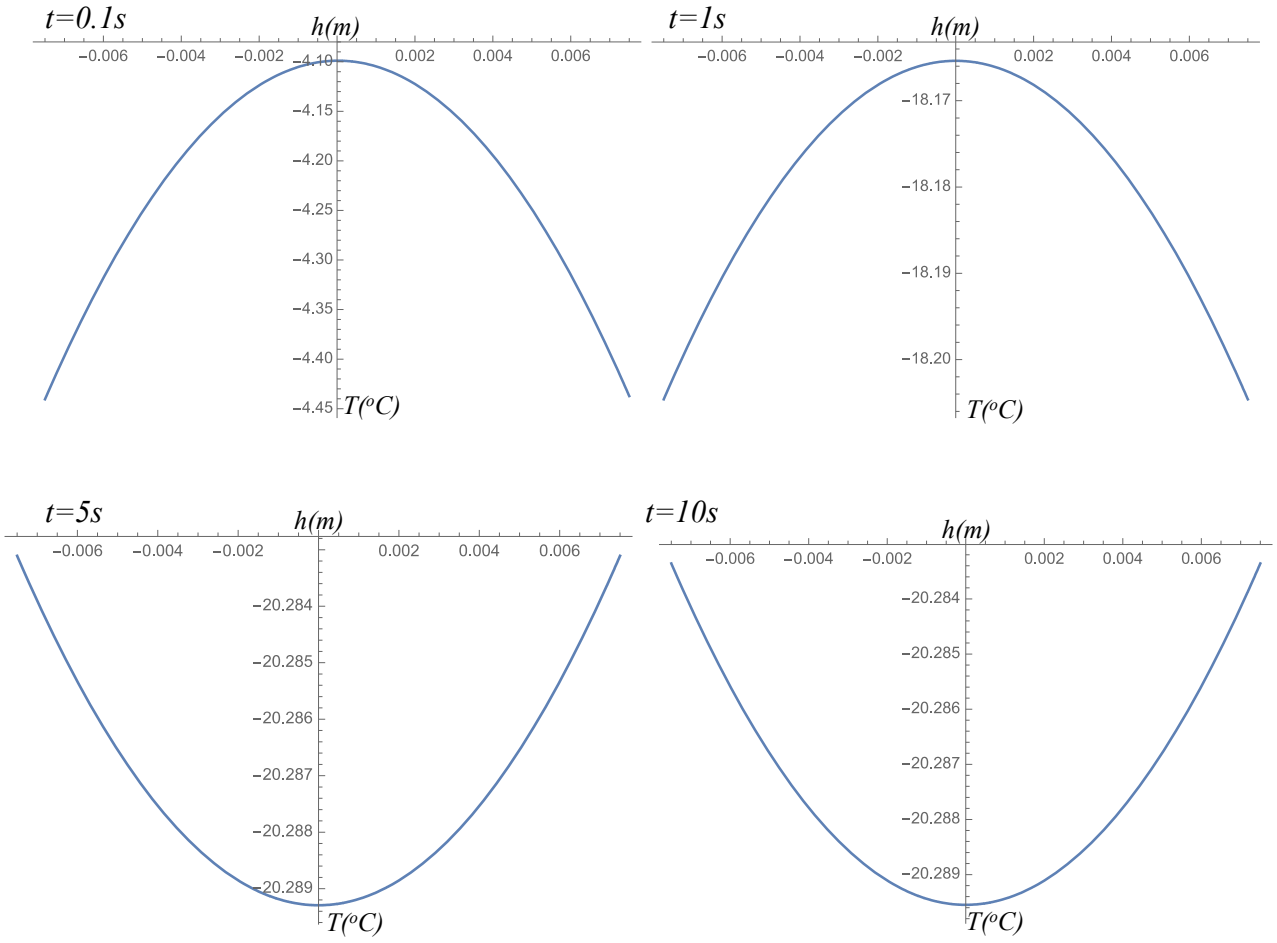

Fig. A4. Temperature distribution across the thickness of the panel (x coordinate) when the panel is under dynamic mechanical loading and in an environmental soak temperature of −20 °C, presented at different instants in time.

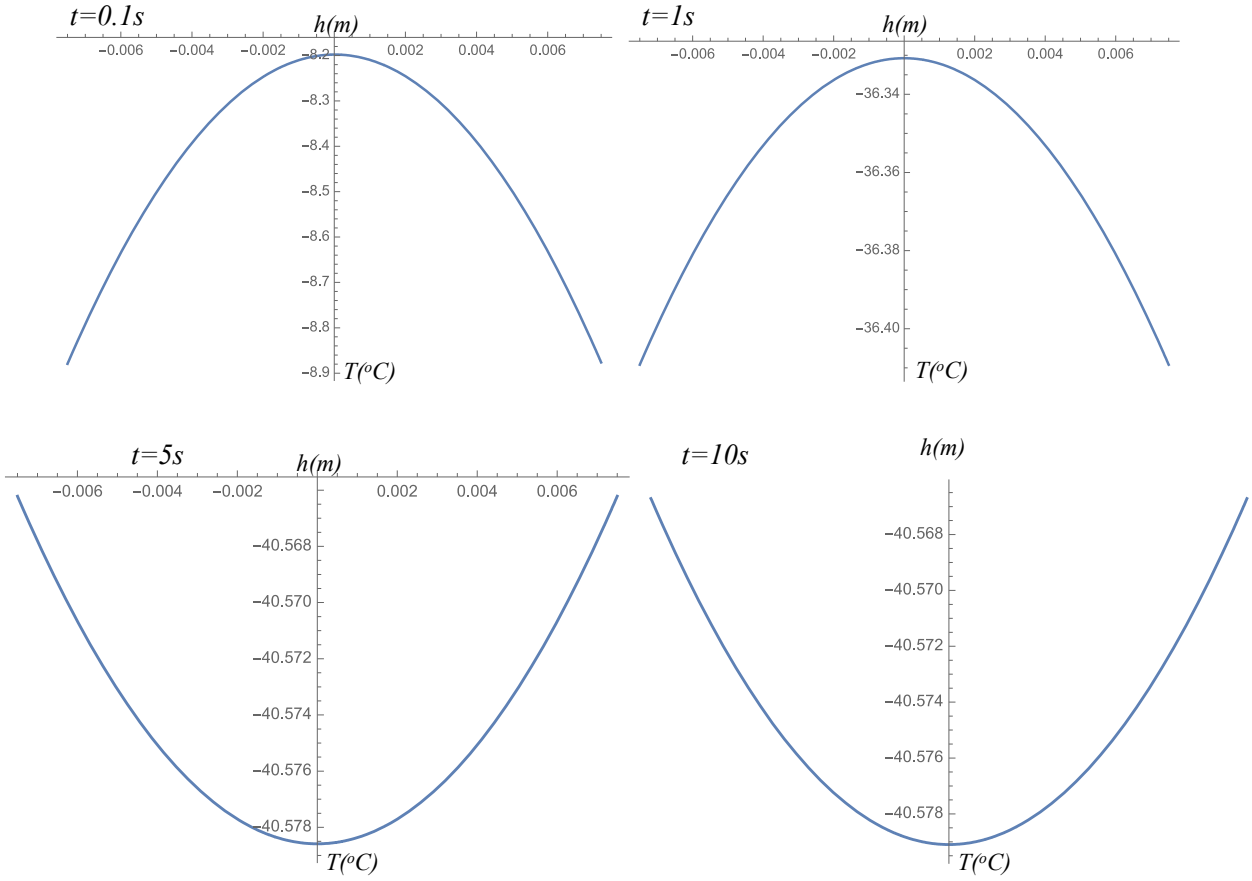

Fig. A5. Temperature distribution across the thickness of the panel (x coordinate) when the panel is under dynamic mechanical loading and in an environmental soak temperature of −40 °C, presented at different instants in time.

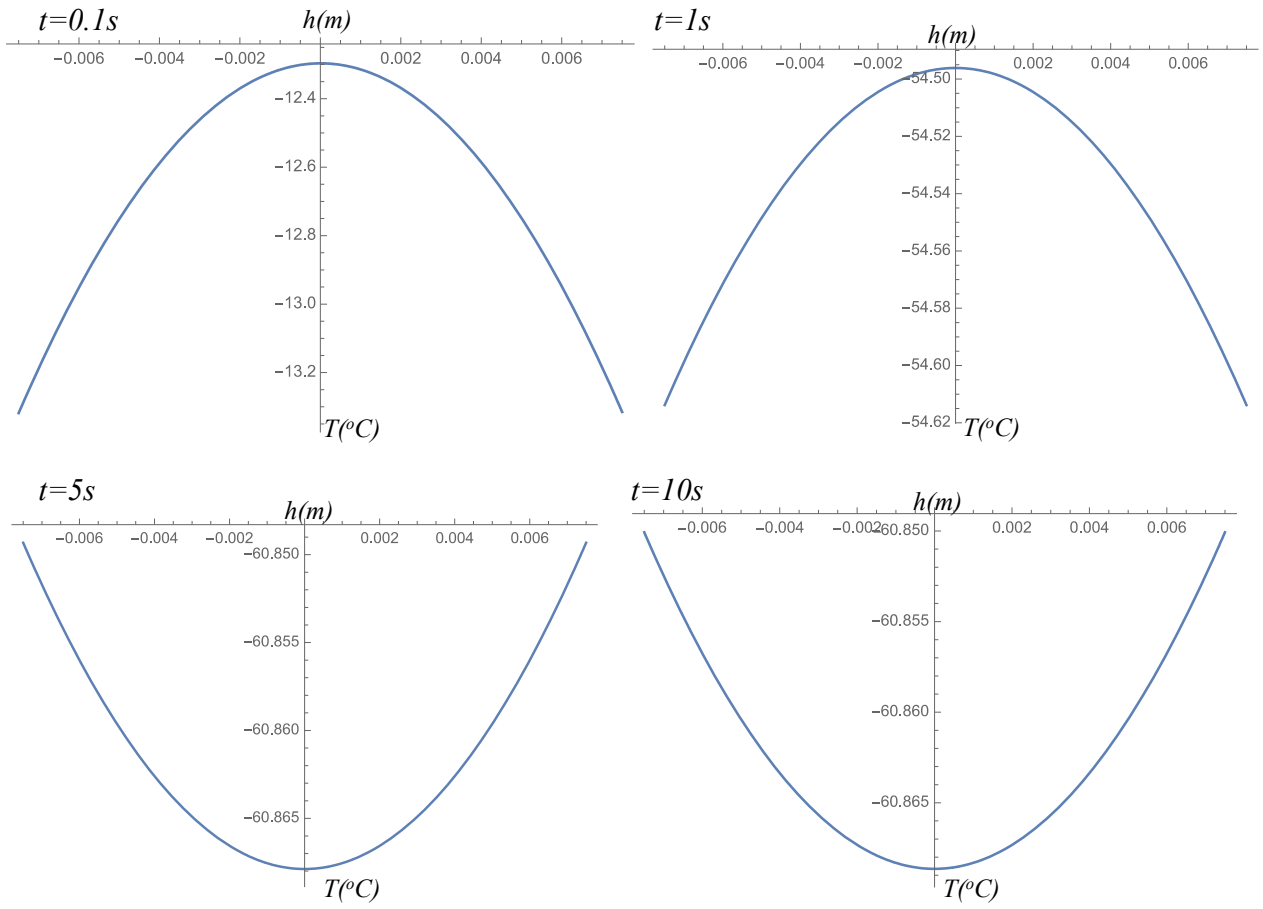

Fig. A6. Temperature distribution across the thickness of the panel (x coordinate) when the panel is under dynamic mechanical loading and in an environmental soak temperature of −60 °C, presented at different instants in time.

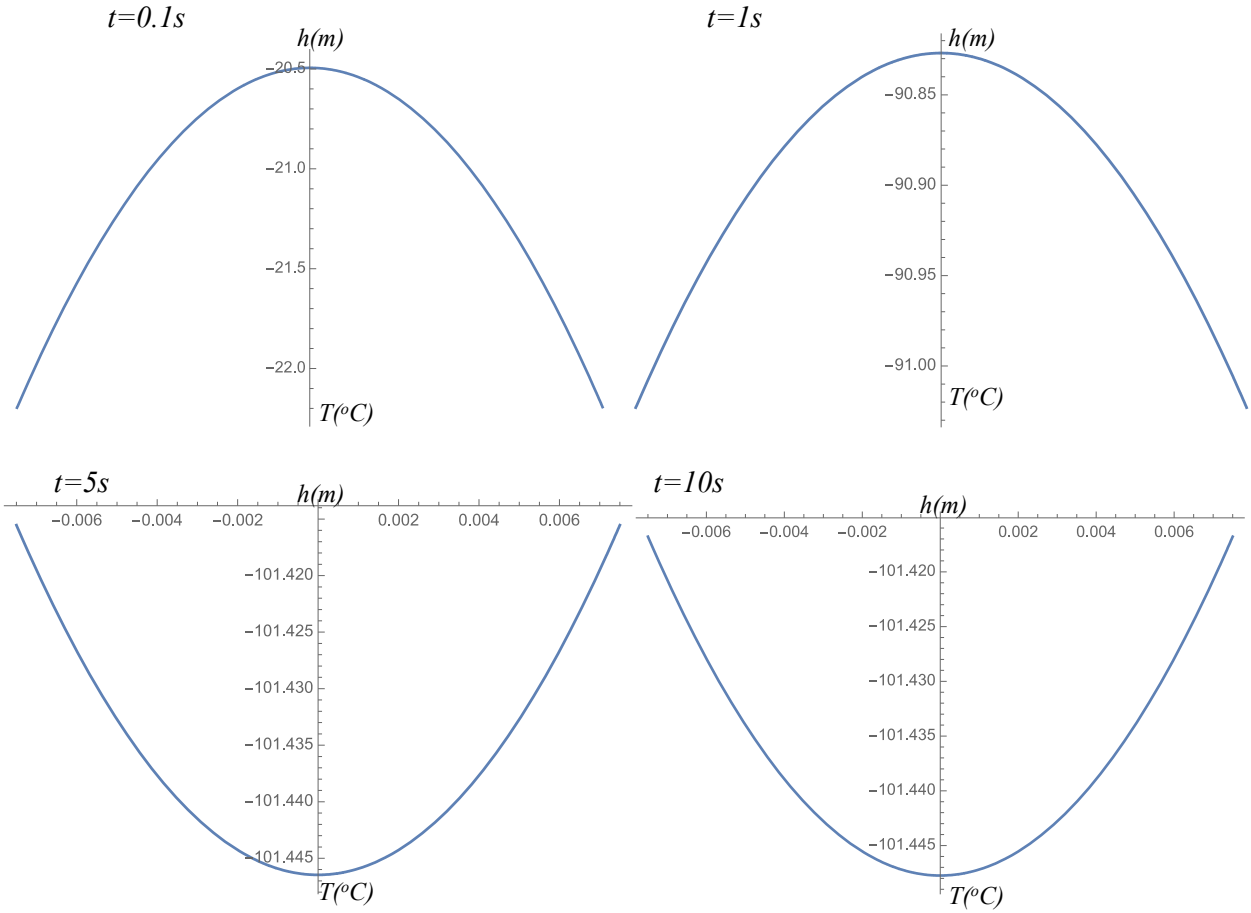

Fig. A7. Temperature distribution across the thickness of the panel (x coordinate) when the panel is under dynamic mechanical loading and in an environmental soak temperature of −100 °C, presented at different instants in time.

References

[1] Finckenor MM, De Groh KK. A Researcher's guide to space environmental effects. International Space Station. NASA. NP-2015-03-015-JSC; 2016. Available at: https://www.nasa.gov/connect/ebooks/researchers_guide_space_environment_detail.html (accessed 13 August 2020).

[2] Clawson JF, Tsuyuki GT, Anderson BJ, Justus CG, Batts W, Ferguson D, et al. Spacecraft thermal Environments. Spacecraft Thermal Control Handbook, Volume I: Fundamentals Technologies. 2nd ed. El Segundo, California: Aerospace Press; 2003.

[3] Bai JB, Shenoi RA, Xiong JJ. Thermal analysis of thin-walled deployable composite boom in simulated space environment. Compos Struct 2017;173:210–8.

[4] Lv P, Zhang Z, Wang X, Ji L, Hou X, Guan Q. Microstructure Evolution of 2024 and 7A09 Aluminium Alloys Subjected to Thermal Cycling in Simulated LEO Space Environment. Mater Res Innovations 2014;18(3):169–75.

[5] Shin K-B, Kim C-G, Hong C-S, Lee H-H. Prediction of Failure Thermal Cycles in Graphite/Epoxy Composite Materials under Simulated Low Earth Orbit Environments. Compos B Eng 2000;31(3):223–35.

[6] Park SY, Choi HS, Choi WJ, Kwon H. Effect of Vacuum Thermal Cyclic Exposures on Unidirectional Carbon Fiber/Epoxy Composites for Low Earth Orbit Space Applications. Compos B Eng 2012;43(2):726–38.

[7] Nowacki W. Thermoelasticity. Pergamon press; 1986.

[8] Brischetto S, Carrera E. Coupled thermo-mechanical analysis of one-layered and multilayered plates. Compos Struct 2010;92(8):1793–812.

[9] Cetkovic M. Thermo-mechanical bending of laminated composite and sandwich plates using layerwise displacement model. Compos Struct 2015;125:388–99.

[10] Caliri MF, Ferreira AJM, Tita V. A review on plate and shell theories for laminated and sandwich structures highlighting the Finite Element Method. Compos Struct 2016;156:63–77.

[11] Cho M, Oh J. Higher order zig-zag theory for fully coupled thermo-electric-mechanical smart composite plates. Int J Solids Struct 2004;41(5-6):1331–56.

[12] Carrera E. Historical review of zig-zag theories for multilayered plates and shells. Appl Mech Rev 2003;56(3):287–308.

[13] Saetta E, Rega G. Third order thermomechanically coupled laminated plate: 2D nonlinear modeling, minimal reduction, and transient/post-buckled dynamics under different thermal excitations. Compos Struct 2017;174:420–41.

[14] Paik J, Thayamballi A, Kim G. The Strength Characteristics of Aluminium Honeycomb Sandwich Panels. Thin-Walled Struct 1999;35(3):205–31.

[15] Abbadi A, Koutsawa Y, Carmasol A, Belouettar S, Azari Z. Experimental and Numerical Characterization of Honeycomb Sandwich Composite Panels. Simul Model Pract Theory 2009;17(10):1533–47.

[16] Belingardi G, Martella P, Peroni L. Fatigue Analysis of Honeycomb-Composite Sandwich Beams. Compos A Appl Sci Manuf 2007;38(4):1183–91.

[17] Ganilova OA, Cartmell MP, Kiley A. Experimental investigation of the thermoelastic performance of an aerospace aluminium honeycomb composite panel. Compos Struct 2021;257:113159. https://doi.org/10.1016/j.compstruct.2020.113159.

[18] HexWeb^{TM} Honeycomb Sandwich Design Technology, December 2000, Publication No. AGU 075b, Hexcel Standard.

[19] CR III. Corrosion Resistant Specification Grade. Aluminum Honeycomb. Product data. 1998 Hexcel Standard.

[20] Brischetto S, Carrera E. Thermomechanical effect in vibration analysis of one-layered and two-layered plates. Int J Apple Mech 2011;03(01):161–85.

[21] Saetta E, Rega G. Unified 2D continuous and reduced order modeling of thermomechanically coupled laminated plate for nonlinear vibrations. Meccanica 2014;49(8):1723–49.

[22] Yeh Y-L. Chaotic and bifurcation dynamic behavior of a simply supported rectangular orthotropic plate with thermo-mechanical coupling. Chaos Solut Fract 2015;24:1243–55.

[23] Saetta E, Rega G. Supplementary Data. Compos Struct 2017. https://doi.org/10.1016/j.compstruct.2017.03.048.

[24] Saetta E, Rega G. Modeling, dimension reduction, and nonlinear vibrations of thermomechanically coupled laminated plates. Procedia Eng 2016;144:875–82.

[25] Ganilova OA, Cartmell MP, Kiley A. The development of a dynamic coupled model for aluminium composite sandwich plates under thermo-elastic loading. Proceedings of the Second International Nonlinear Dynamics Conference, NODYCON2021, Rome, Italy, 16 - 19 February 2021, Publication Date September 2021.

[26] Ganilova OA, Cartmell MP, Kiley A. Open Data for the paper 'Experimental investigation of the thermoelastic performance of an aerospace aluminium honeycomb composite panel'. University of Strathclyde; 2019.